2020

Development of a Platform for the Biofabrication of Endocrine Pancreatic Tissue Constructs through Co-Axial Micro-Extrusion

Max Jurie Renes
The University of Wollongong

UNIVERSITY
OF WOLLONGONG
AUSTRALIA

Development of a Platform for the Biofabrication of Endocrine Pancreatic Tissue Constructs through Co-Axial Micro-Extrusion

Max Jurie Renes

Supervisors:

Dr. Xiao Liu

Dr. Zhilian Yue

Prof. Gordon G. Wallace

This thesis is presented as part of the requirement for the conferral of the degrees:

Master of Philosophy, Biofabrication, University of Wollongong

Master of Science, Biofabrication, Utrecht University

The University of Wollongong

Intelligent Polymer Research Institute (IPRI)

Australian Institute of Innovative Materials (AIIM)

March 2020

I. Abstract

Type-1 Diabetes (T1D) is an auto-immune disease in which the insulin-producing β-cells in the islets of Langerhans are destroyed, affecting over 20 million patients worldwide. Islet transplantation may offer a viable treatment strategy, but transplanted islet lifespan is limited by auto- and allo-immune responses and poor engraftment upon transplantation. Biofabrication of tissue engineered constructs encapsulating islets may offer a viable strategy, as this encapsulation may allow for immune-protection of the islets and circumvent issues associated with engraftment. Here, we describe for the first time a single-step fabrication procedure for tissue constructs incorporating isolated mouse islets with supporting endothelial progenitor cells. A platform for the fabrication of these constructs through co-axial micro-extrusion (Dual Ink Co-axial Bioprinter-1; DICAB-1) was first established, characterised and found to be biocompatible with MS1 and β-TC-6 cell lines (endothelial and beta-cells of murine origin, respectively). Bioprinted islets were found to survive fabrication procedures as well as secrete considerable amounts of insulin, albeit with substantial variability and with sub-optimal glucose responsivity. These results constitute a major step towards the development of a sophisticated platform in which constructs incorporating islets, supporting cells and immune protection can be fabricated in a single-step process.

II. Acknowledgments

I would like to acknowledge and express my gratitude in the first place to my supervisors, Zhilian, Xiao and Gordon, for their help and guidance and the role they played in making this project possible. Furthermore, I would like to thank the collaborators at the University of Adelaide in the group of Professor Coates, for allowing me to conduct several of the key experiments of this thesis and for their assistance along the way. I would like to thank Juewan Kim for assistance with flow cytometry and Daniella Penko for the islet and EPC isolations. Furthermore, I would like to thank Sarah Carter, the student previously involved in this project, for her work developing and characterising the bioink and providing me with helpful advice at the start of the project. I would like to thank Cameron Angus and Dr. Stephen Beirne, for the development of the DICAB-1 and continuous technical support. Finally, I would like to thank all the members and founders of the international Biofabrication Master's degree, in particular from the University of Wollongong and Utrecht University, as this programme and thereby this thesis would never have been a reality without it.

III. Certification

I, Max Renes, declare that this thesis submitted in fulfilment of the requirements for the conferral of the degree Biofabrication, Master of Philosophy, from the University of Wollongong, is wholly my own work unless otherwise referenced or acknowledged. This document has not been submitted for qualifications at any other academic institution, with the exception of the international double Master's degree in Biofabrication at Utrecht University, in line with the curriculum of the degrees.

_____

Max Jurie Renes

01-07- '18

Biofabrication double degree statement

Appended to this document (Appendix 3) is an additional annex that represents the entirety of a one-year project undertaken at the Utrecht University and submitted as part of the fulfilment of the Double Degree Masters of Biofabrication between the UOW and Utrecht.

According to the Memorandum of Agreement between: Queensland University of Technology, University of Wollongong, Julius-Maximilians-Universität Würzburg and Utrecht University, the Biofabrication Double degree master's program was started.

Students in the programme will be expected to obtain a Master's degree from one European and one Australian institution. The student initiates the Biofabrication Mobility Programme in a Master's degree at the home institution for two semesters (60 EC in Europe) over one year, prior to taking up enrolment in another Master's degree at the overseas participating institution, hereinafter referred to host institution for a period of two semesters (60 EC in Europe) over one year.

Students shall enrol in a Master's degree at the home institution in accordance with the Biofabrication Mobility Programme specifications approved jointly by the institutions. Students will undertake a research project at the host institution in accordance with the project descriptions provided by each institution (supervisory and infrastructure capacity).

IV. List of Abbreviations

AM	Additive Manufacturing
CAD	Computer-Aided Design
CI	Confidence Interval
DICAB-1	Dual Ink Co-Axial Bioprinter 1
ECM	Extra-Cellular Matrix
ELISA	Enzyme-Linked Immuno-Sorbent Assay
EPC	Endothelial Progenitor Cell
ESC	Embryonic Stem Cell
FBS	Foetal Bovine Serum
FDA	Fluorescein Diacetate
FDM	Fused Deposition Modelling
GelMA	Gelatine Methacryloyl
GSIS	Glucose Stimulated Insulin Secretion
iPSC	Induced Pluripotent Stem Cell
LAP	Lithium phenyl-2,4,6-trimethylbenzoylphosphinate (photo-initiator)
MS1	Mile Sven 1
PBS	Phosphate-Buffered Saline
PI	Propidium Iodide
PLA	Poly-lactic Acid
RT	Room Temperature
SD	Standard Deviation
T1D	Type-1 Diabetes
T2D	Type-2 Diabetes
T3cD	Type-3c Diabetes
TE	Tissue Engineering
T-reg	Regulatory T-cells
VEGF	Vascular Endothelial Growth Factor

V. Table of Contents

_Toc520146528

VI. Layman's Summary

Type-I diabetes (T1D) affects over 20 million people worldwide. In T1D, the body cannot produce enough insulin, which is important for regulating blood sugar. This is caused by the destruction of the β-cells that produce insulin by the patient's own immune system in an auto-immune reaction. These β-cells are located in the islets of Langerhans. Therefore, one potential treatment is the transplantation of islets from donors to patients suffering from T1D. However, the wide-spread use of this treatment is hindered by a shortage in donor islets, and because the transplanted islets tend to die over time due to rejection or the auto-immune response.

A possible solution is therefore to encapsulate the islets in a material that protects them, but at the same time still allows for the release of insulin. To release insulin, it is important that the blood is still able to reach the islets which also supplies oxygen and nutrients to the islets. Therefore, a platform has been developed here for 3D-printing constructs with islets and blood vessel cells, which may meet these requirements. The constructs were printed with a new, custom-designed 3D-printer: the DICAB-1 (Dual Ink Co-Axial Bioprinter).

DICAB-1 can print two materials (or cell types) at the same time into core and shell fibres. This was first confirmed with a simple gel and next with a cell-friendly bioink. It was then demonstrated that the platform could print core/shell-fibres with β-cells and blood vessel cells and that the cells survived the process. In a final set of experiments, it was investigated whether the DICAB-1 could print mouse islets and blood vessel progenitor cells. It was established that islets as well as these blood vessel progenitor cells also survived the printing and that the islets released insulin. However, it was also seen that the islets in these constructs did not match the natural insulin release response, which may be improved in a more complex print design which has been described here as well.

Chapter 1

1. Introduction

Type-I diabetes (T1D) is an auto-immune disease that affects the pancreas and is characterised by the patient's inability to produce (sufficient) insulin, which consequently affects blood glucose homeostasis. In 2014, it was estimated to affect over 20,000,000 patients worldwide.[1] Long-standing T1D is associated with various major complications with considerable morbidity and mortality, including cardiovascular disease, stroke, blindness, kidney disease and ketoacidosis.[2–5] In spite of significant effort and progress in treatment and management, still no effective cure or preventative measure exists for T1D.[5]

In this respect, Tissue Engineering (TE) may offer a viable strategy. TE aims to fabricate tissue constructs in order to replace or repair diseased tissue and restore its function. TE has been applied with some clinical success for instance in the regeneration of skin[6], urethra[7] and cartilage[8]. TE has also shown potential for the treatment of T1D through the fabrication of endocrine pancreatic constructs.[9,10] However, the field still faces several challenges in this area, some of which are associated specifically with T1D. A major hurdle that still needs to be overcome in TE for almost all applications is the development of proper vascularisation in tissue constructs. This is essential for the supply of nutrients and oxygen throughout the construct while simultaneously removing waste products.[11,12] Specifically for T1D, another obstacle is associated with the mechanism of the disease. It is required that the tissue construct is in some way protected from the host immune system in order to prevent auto-immune destruction, in addition to immune rejection of implanted materials or tissues that may affect TE constructs in general.

Within TE, the recent science of Biofabrication is one of the most promising strategies for the fabrication of tissue constructs. It has been defined as "the automated generation of biologically functional products with structural organisation from living cells, bioactive molecules, biomaterials, cell aggregates such as micro-tissues, or hybrid cell-material constructs, through Bioprinting or Bioassembly and subsequent tissue maturation processes".[13] Informally, it is commonly used to refer to the application of Additive Manufacturing (AM; '3D-printing') of cells and/or biomaterials to fabricate tissue constructs.

This thesis is a report of a project dedicated towards the Biofabrication of endocrine pancreatic constructs. In the first following chapter, the focus will be on providing a framework of the mechanisms behind T1D, current treatments and background on TE and Biofabrication of endocrine pancreatic constructs. Then, the aims of the project and the developed platform will be outlined and the obtained results will be presented and discussed. Finally, a reflection on the project will be offered with a future outlook.

Chapter 2

2. Background

2.1 The pancreas and Type-I Diabetes

The pancreas is a small organ situated behind the stomach in the abdominal cavity. It has major exocrine as well as endocrine functions. The exocrine functions of the pancreas mainly consist of the secretion of pancreatic juice into the duodenum, which contains both essential digestive enzymes as well as ions to neutralise the pH of the chime entering the intestine. The endocrine functions of the pancreas consist of the release of several hormones, which are required to maintain homeostasis. These include insulin, glucagon and somatostatin, all of which are released into the bloodstream. Insulin, the hormone that is most relevant here, is essential for the uptake and anabolism of glucose into for example glycogen in liver and muscles.[5,14]

In T1D, the synthesis and secretion of insulin is impeded. This is due to an auto-immune response towards the insulin-producing β-cells in the Islets of Langerhans. The immune response is mounted by a combination of autoreactive CD4+ and CD8+ T-lymphocytes, autoantibody producing B-lymphocytes as well as various activated parts of the innate immune system. The exact causes of the auto-immunity are not fully understood, but it is thought to be a combination of hereditary and environmental factors.[5,15] In spite of the importance of the endocrine functions of the β-cells in the islets of Langerhans, they possess strongly limited regenerative potential which further declines with increasing age.[16,17] As such, once β-cells are depleted, they are not naturally replenished and if left entirely untreated T1D is ultimately fatal due to the inability to maintain normoglycaemia (normal blood glucose levels).

2.2 Current treatment and therapy

Current treatment for T1D consists of the administration of exogenous recombinant insulin, which is required for patient survival. This can either occur via regular injection, or via an insulin pump.[18] Although this treatment offers some degree of control over of blood glucose levels, a long-term risk for severe complications is still present in patients undergoing treatment. These potential complications include cardiovascular disease, stroke, blindness, kidney disease and ketoacidosis.[2–5] Moreover, patients are prone to develop insensitivity to life threatening hypoglycaemia (low blood sugar).[19–21] The necessity of regular injections or the insulin pump additionally constitute therapies that are considerably invasive and have a major impact on the daily life of the patients. As a final consideration, both therapies are also sub-optimal in that they fail to mimic the fine-tuned, glucose-responsive natural secretion dynamics of the β-cells in the pancreas.[22]

A potential alternative treatment is whole organ pancreas transplantation which may restore long-term normoglycaemia. This is however an invasive procedure and exposes patients to considerable surgical risk. Patients furthermore require lifelong immune-suppressants. As a consequence, whole organ pancreas transplantation is commonly limited to patients who

additionally require kidney transplants which already necessitate the use of immune-suppressants and invasive surgery.[23,24] In patients with adequate kidney function, the potential benefits of whole organ transplantation may therefore not outweigh the risks.[25]

As such, transplantation of pancreatic islets has been investigated and used as a potential alternative.[26] In 2000, islet transplantation gained momentum with the establishment of the Edmonton protocol[27], where considerable clinical success had been achieved with transplanted islets in combination with immune-suppression. Patients did not require exogenous insulin administration for an average of one year after transplantation. As a major advantage over whole organ transplantation, islet transplantation can be performed with minimally invasive surgery with minimal morbidity and risk of infection.[28] However, there are some issues with the transplantation of islets. In addition to immunogenic rejection associated with transplantation (the allo-immune response), the auto-immune response poses an additional mechanism through which the immune system will reduce the effectivity of transplanted islets over time. As a consequence, in the original study of the Edmonton protocol all donor islet function was lost in all patients after 2 years post transplantation.[27]

In order to improve the life span of these islets, extensive research has been conducted to establish various strategies to protect transplanted islets from auto-immune destruction and allo-immune rejection.[29,30] These will be reviewed at length further below. However, an additional factor is the general shortage in the availability of donor pancreata and islets, which further prevents wide-scale application. Tissue Engineering (TE) may be a suitable strategy to combat both these challenges in two ways: by designing constructs in which β-cells are protected from immune responses and by designing solutions to circumvent the shortage in allogeneic islets.

2.3 Tissue engineering for Type-I Diabetes

There are three requirements that a successful tissue construct for T1D must meet (**Fig. 1**). First and foremost, there is the central clinical requirement: the cells or islets in the construct must establish reliable insulin secretion in response to high blood glucose levels (glucose stimulated insulin secretion; GSIS). For optimal GSIS, the primary concern is a reliable islet or β-cell source which possesses sufficient GSIS potential. The second requirement for a tissue construct is that it must protect the insulin-producing cells from the allo- and auto-immune reaction to prevent degradation. Third, it must allow for the diffusion of nutrients and oxygen into the construct to maintain cell viability and allow for the removal of waste products, potentially through the development of vascularisation. This will also be required for the detection of blood glucose levels for GSIS and the transport of that insulin into the host circulatory system. All these requirements will be highlighted individually below.

2.3.1 Cell sources and GSIS

The first consideration in optimising GSIS is the cell source for the tissue construct. For TE in general, cells can be derived from cell lines, (induced) stem cells or primary cells.[31] One limiting factor in the application of primary cells is that there is currently insufficient donor tissue available to act as a large-scale cell source. An additional limiting factor is that isolated islets and β-cells tend to lose function and de-differentiate in *in vitro* culture.[32,33]

This de-differentiation *in vitro* has also long been an issue for establishing reliable β-cell lines. Recently, some strains have been developed that show more reliable GSIS[34,35], but it will likely still be insufficient for applications past model systems. Although of value for fundamental research, cell lines are also unsuitable for clinical application due to their unlimited proliferation. Hence, research has focused on alternative cell sources that may be relevant for clinical application. Most notably, these include xenogeneic β-cells and islets[36] or (induced) stem cells (re-) differentiated towards β-cell phenotype.[37]

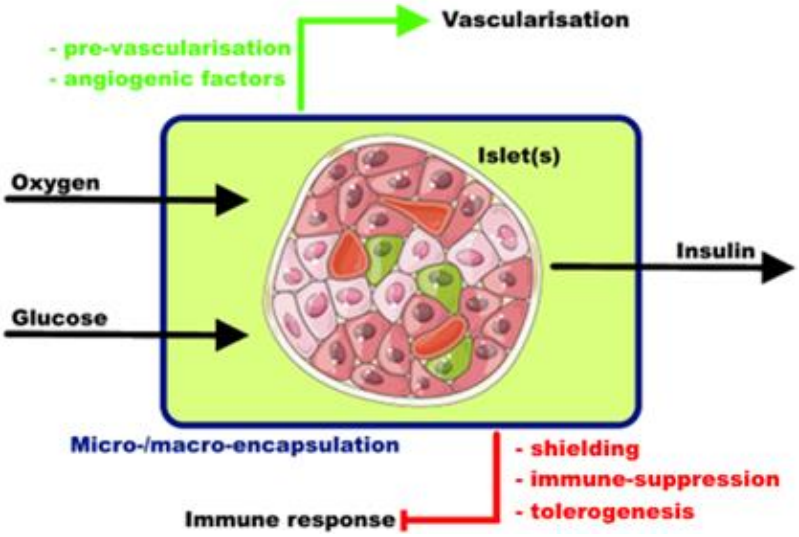

Fig. 1: A schematic representation of the complex set of requirements for an optimal tissue engineered construct for T1D. If present, micro- or macro-encapsulation should allow for influx of oxygen and nutrients; most importantly glucose to allow for detection of blood glucose levels. Additionally, the construct should in some way protect the β-cells or islets from the host immune response. Finally, it should allow for the secretion of insulin. Therefore, it must support the development of vascularisation. Image partially adapted from Servier Smart Medical Art (ref. 121).

Primary β-cells or islets derived from porcine origin have been investigated most notably as a potential xenogeneic cell source, as porcine insulin and β-cells are highly similar to the human equivalents.[37,38] For these cells, supply could be sufficient to meet clinical needs. There has been some clinical success using β-cells from porcine origin[36,39], and some of the major issues in terms of xenogeneic acute rejection may be resolved through genetic engineering[40]. Some of the remaining drawbacks include potential zoonosis of diseases (such as porcine endogenous retroviral (PERV) sequences)[41] and patients may oblige to xenotransplantation for ideological reasons.

Alternatively, insulin-producing cells can be obtained from differentiation of stem cells

towards β-cell phenotype. Of particular interest are the recent developments in the formation of islet-like cell clusters (or pseudo-islets). Embryonic stem cells (ESCs)[42,43] or induced pluripotent stem cells (iPSCs)[44,45] could both be suitable cell sources to this end. Major steps have been made in this field recently, and pseudo-islets that possess reliable GSIS have been generated from both ESCs and iPSCs. However, there are still several issues in terms of the full maturation of the stem cells. Not all mechanics and factors behind the maturation of these cells are understood yet, thus the generated cells still differ somewhat in insulin secretion dynamics from fully developed β-cells *in vivo*.[46,47] Although some of the ethical issues associated with the use of ESCs can be circumvented through the use of iPSCs, there are still major concerns around the possibility of teratoma formation.[47] As a final (stem) cell source, mesenchymal stromal cells have also been investigated for differentiation towards insulin producing cells, but with limited success. They may, however, be useful as supporting cells.[48,49]

It has been established that the environment of the β-cells has a major impact on their performance in GSIS. TE constructs employing biomaterials that closely resemble the natural extra-cellular matrix (ECM) may therefore enhance GSIS for any cell source. However, it has been shown furthermore that the surrounding cells in pancreatic islets, such as α-, δ- and endothelial cells, all play a role in regulating β-cell function.[50] As such, whole islets still possess the most reliable GSIS, especially over individual β-cells.[51–53] The main focus here will thus be on TE with whole pancreatic islets. It can be noted, however, that most strategies described here for islets could be applied for stem cell-derived pseudo-islets as well.

2.3.2 Protection from the host immune system

The second requirement for a successful TE pancreatic construct is the protection of the β-cells from the host immune response. Protection from the immune system will greatly increase the lifespan of a construct by avoiding allo- and auto-immune destruction. In addition, it may resolve some of the risks associated with the use of any allo-or xenogeneic cells. There are three distinct strategies to achieve such protection: shielding, immune-suppression and tolerogenesis. In the former, transplanted islets are attempted to be 'hidden' from the host immune system by a physical barrier, avoiding contact with the host immune system altogether. The second, immune-suppressive protection, is currently used most commonly and relies on the (systemic) suppression of immune responses through administration of immunosuppressive drugs. Finally, in tolerogenic approaches, it is attempted to sway the host immune system towards tolerance of the construct.

Within immune-shielding, there are mainly two different strategies that are being employed to achieve protection from the host immune system: micro- and macro-encapsulation. The former refers to the encapsulation of individual or small amounts of islets; the latter refers to the encapsulation of a multitude of islets into one construct or in a more macroscopic, device-like set-up or bio-artificial pancreas.

Both micro-encapsulation as well as macro-encapsulation have been employed with varying

degrees of success.[30,54] Various materials have been used for the micro-encapsulation of islets, but alginate has by far been investigated most extensively.[55] This strategy has led to several clinical trials. In the first clinical trial in 1994, insulin independence was achieved for 9 months[56], albeit in combination with immune-suppressants for a previous kidney transplant. A primary goal of the encapsulation is, however, to avoid the use of immune-suppressants altogether. Conversely, most micro-encapsulated islets that do not require immune-suppressants have failed to achieve insulin independence in the clinic.[55,57–59]

A major advantage of macro-encapsulation is that the device can be retrieved upon complications due to for example infection. Macro-encapsulation requires complex design, however, in order to allow for the passage of glucose and insulin while blocking cellular and humoral immune agents.[60,61] To this extent, silicon semi-permeable membranes have been developed with pore sizes that fit this narrow window[60,62] and recently this has been achieved with polycaprolactone (PCL)[63]. A larger construct as a result of macro-encapsulation may potentially exclude the use of minimally invasive surgery, however, and increase fibrotic overgrowth or foreign body responses[61].

Immune-suppressive therapy is the current gold standard protection from host immune-system. It increases the lifespan of non-encapsulated, transplanted islets[27,64,65], but there are considerable drawbacks to their extensive use. They render patients more vulnerable to infection and many immune-suppressants are toxic to β-cells, affecting their function. In fact, they possess substantial toxicity in general and lead to major patient discomfort, with established side-effects including mouth and duodenal ulceration and bleeding, anaemia, leukopenia, nausea, vomiting and increased risk of certain cancers.[55,66,67] There is a large array of different immune-suppressants with different working mechanisms, but a combination of various drugs is often required. Reviewing all here is beyond the scope of this thesis, but excellent recent reviews[61,64] of their use in relation to islet transplantation are available.

The final option for protection against host immune responses is the induction of (local) tolerance to the construct. Tolerogenesis may circumvent most of the drawbacks associated with immune-suppressants, as it can be induced locally and specifically instead of systemically. It may be achieved through for example sustained release of anti-inflammatory cytokines or co-transplantation of (β-cell specific) regulatory T-cells (T-regs). T-regs have previously been shown to be safe for human transplantation and are currently used in early phase clinical trials for T1D patients, further demonstrating the feasibility of this approach.[68,69]

The various approaches for immune-protection are not necessarily mutually exclusive. On the contrary, macro- and micro-encapsulated islets are commonly still used in combination with immune-suppressive drugs. Alternatively, constructs that provide encapsulation could be additionally designed to accommodate tolerogenic agents. It is however unlikely that immune-suppression and tolerogenesis are easily compatible. Several immune-suppressants aspecifically

downregulate T-lymphocytes and thereby T-regs or otherwise impede T-reg function.[61] As such, this may interfere with the induction of tolerance and combinations of both (systemic) immune-suppression and tolerogenesis may be difficult. Optimal tolerogenesis should nonetheless avoid the necessity of immune-suppressants, and considering the serious side-effects of immune-suppression, tolero-genesis may be a preferred strategy when feasible.

2.3.3 Vascularisation and delivery of nutrients and oxygen

A final requirement for the success of TE pancreatic constructs is the delivery of nutrients and oxygen throughout the constructs, while removing toxic waste.[11,12] Mere diffusion is commonly insufficient: the maximum construct thickness for which diffusion would be sufficient is limited to 200 μm[70]; larger constructs are known to develop a necrotic core due to the lack of oxygen and nutrients.[71] Thus, TE constructs require some form of (pre-)vascularisation to reach more clinically relevant sizes without necrosis. Given the high metabolism of β-cells and necessity of secreting insulin into the bloodstream, vascularisation is of particular importance for TE with pancreatic islets. This is further signified by the fact that around 10% of islet volume consists of vasculature[72], which is additionally over 10 times more fenestrated than in the exocrine pancreas.[72,73]

To achieve vascularisation, a multitude of strategies could be employed. This will only be briefly touched upon here, as these recently have been reviewed by the same author of this thesis.[74] One option is to integrate perfusable channels in the tissue construct, which could serve to supply nutrients throughout the construct during *in vitro* culture.[75,76] At a later stage, these channels could be lined with endothelial (progenitor) cells in order to form blood vessel-like structures. Another option is patterned pre-vascularisation which may be obtained through co-culture of β-cells or islets with endothelial cells.[77] Both options can be further stimulated through the administration of growth factors, such as vascular endothelial growth factor (VEGF).[78] Following either option, the construct is likely to have an increased lifespan upon *in vivo* transplantation, when the vessel network anastomoses with the host circulation.

2.4 Biofabrication and co-axial micro-extrusion

It is evident that intelligent construct design is essential, considering the number and the complexity of the requirements for an optimal, tissue engineered endocrine pancreatic construct. In this respect, Biofabrication holds substantial promise as a method. The hallmark properties of Biofabrication include the ability to fabricate TE constructs of customised, complex architectures designed through Computer Aided Design (CAD). These can be fabricated with superior spatial control, which is inherently associated with AM. At the same time, Biofabrication can still offer the general benefits of TE and 3D-cell culture through the use of ECM-resembling biomaterials and growth factors, albeit that some cell viability may initially be lost in the printing process.[13,79] Several different printing techniques are currently employed in Biofabrication, each associated with a set of (dis)advantages that renders different printing techniques suitable for different applications. Reviewing all of these techniques is beyond the scope of this thesis and several excellent reviews are available on this

topic.[13,31,79,80] Rather, only the method employed in this project will be highlighted and attention will be paid to some interesting recent developments that are relevant to this project.

One of the most commonly employed methods for 3D-Bioprinting is micro-extrusion (**Fig. 2**).[31,81,82] In micro-extrusion, the bioink (the biomaterials and/or cells that are being deposited) is continuously extruded through a nozzle. This leads to deposited fibres of bioink. The force required for the extrusion of this material can be supplied pneumatically (i.e. with air pressure) or mechanically (with a piston or screw). Although pneumatic extrusion can sometimes be inexpensive or easier to implement than mechanical alternatives, it is typically inferior in terms of control and resolution, as the applied force is less defined. The required build-up of air pressure which delays extrusion can furthermore lead to an "overshoot" of material upon initiation of printing. Mechanical set-ups in turn may have a lower maximum applied force, which may be limiting for the deposition of some highly viscous bioinks.[31]

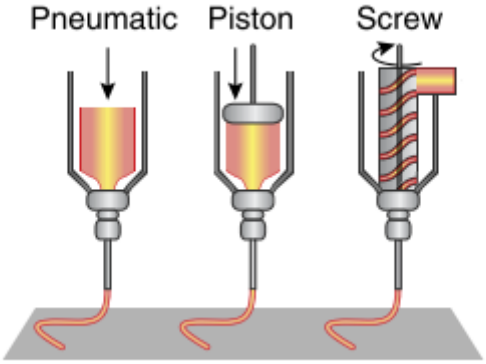

Figure 2: Three distinct, possible mechanisms for supplying the required pressure for micro-extrusion. Micro-extrusion based on a piston and a screw can both be sub-categorised into "mechanical extrusion".

Edited from: Murphy et al. (ref. 31)

Of interest here is the progress that has been made with the development of co-axial micro-extrusion. In these set-ups, at least two concentric nozzles are employed to simultaneously deposit a core material and shell material.[83] This offers the possibility to deposit two different materials or cell types simultaneously in a spatially defined manner, or rapid crosslinking by supplying crosslinker-solution through either nozzle. By running crosslinker solution in the core, it has also been employed in the past to fabricate hollow structures for the fabrication of perfusable channels and/or blood vessels.[84,85]

Biofabrication is not yet widely employed in the field of pancreatic tissue engineering.[10,86–90] Nonetheless, the limited previous instances of Biofabrication for endocrine pancreas tissue engineering will be discussed in the context of the present thesis in the discussion below. One potential additional use of a core/shell-deposition for pancreatic tissue engineering that has not previously been investigated may however be found in the fabrication of constructs with immune shielding. A core material containing the vulnerable β-cells may be printed simultaneously with a shell material that could offer shielding from the host immune system. In such an approach, the β-cells will be protected from degradation while the core encapsulation material can be designed to meet the biological requirements of the cells. This could allow for encapsulation of the β-cells in a more cell-friendly material in the core as this material no longer needs to provide the protection from the immune system.

Chapter 3

3. Project Aim and Platform

3.1 Project aim

In this project, it will be attempted to fabricate endocrine pancreatic tissue constructs encapsulating pancreatic islets through co-axial micro-extrusion. The project is part of an overarching ongoing research programme. The overarching aim of the research at large can be formulated as:

"To establish a platform for the fabrication of endocrine pancreas-like tissue constructs in a co-axial printing set-up, incorporating endothelial cell network formation, which are protected from immune reactions and secrete insulin in response to glucose."

Within this broad framework, the focus of this thesis will be on the optimisation and characterisation of a new, customised printing set-up, establishing its biocompatibility and on the primary endocrine function of the pancreas: the secretion of insulin. The immune-protection and endothelial cell network formation are being investigated in other projects that are currently running in parallel. The platform that has been developed here will be outlined briefly below. Detailed methods and experimental set-up can be found in the Methods section.

3.2 The Platform

3.2.1 The Dual Ink Co-Axial Bioprinter (DICAB-1)

For the fabrication of the tissue constructs, a custom 3D-printer with a co-axial extrusion set-up will be employed (**Fig. 3**). This newly developed printer will be referred to as the DICAB-1 (Dual Ink Co-Axial Bioprinter 1), named for its ability to simultaneously, co-axially extrude a core and a shell fibre. The DICAB-1 features two independent extruders (**Fig. 3B**) which extrude through two concentric nozzles (**Fig. 3CD**) into core/shell-fibres. These extruders each consist of a stepper motor with an 'extruder rod' (consisting of a threaded rod and nut assembly) applying mechanical force to a cartridge in the form of a 1 mL or 3 mL syringe. The syringes are placed in the DICAB-1 behind the 'doors' which contain temperature regulation units. As such, the DICAB-1 could vary the temperature of the cartridge to suit the rheological requirements of various bioinks. The two extruders together with the co-axial nozzles and temperature control units make up the print head which can move independently along two axes: left/right along the x-axis and up/down along the z-axis. The three axes system is completed with movement of the build plate along the y-axis.

In a way, the DICAB-1 can be seen as an automated version of the previously developed Biopen.[91] As such, although the DICAB-1 is the first of its kind developed here, some of its hallmark components have been derived from the Biopen. The most important feature is the custom-manufactured titanium nozzles (through selective laser melting), which are similar to the ones previously developed for the Biopen.[91] However, where initially the Biopen relied on side-by-side

deposition of two materials through co-linear nozzles, the nozzles used here rely on a co-axial configuration which has been derived from later iterations of the Biopen resulting in core/shell deposition (**Fig.3C** and **3D**).[92,93] In the past, these nozzles have been employed in the co-axial melt extrusion of Alginate with PCL[94] as well as fused deposition modelling (FDM) with poly-lactic acid (PLA)[95] and most recently with the Biopen for *in situ* cartilage tissue engineering[92,93]. Notwithstanding the above, the co-linear nozzles mentioned previously would still be compatible with DICAB-1 for other applications beyond the scope of this thesis.

Two different sets of co-axial nozzles were employed for the experiments performed here. For most experiments, co-axial nozzles with a diameter of 449 ± 16 µm for the inner nozzle and a diameter of 1044 ± 24 µm for the outer nozzle were used. For the last set of experiments (see methods), a second set of nozzles was used with an inner and outer nozzle diameter of 502 ± 14 µm and 1241 ± 46 µm, respectively.

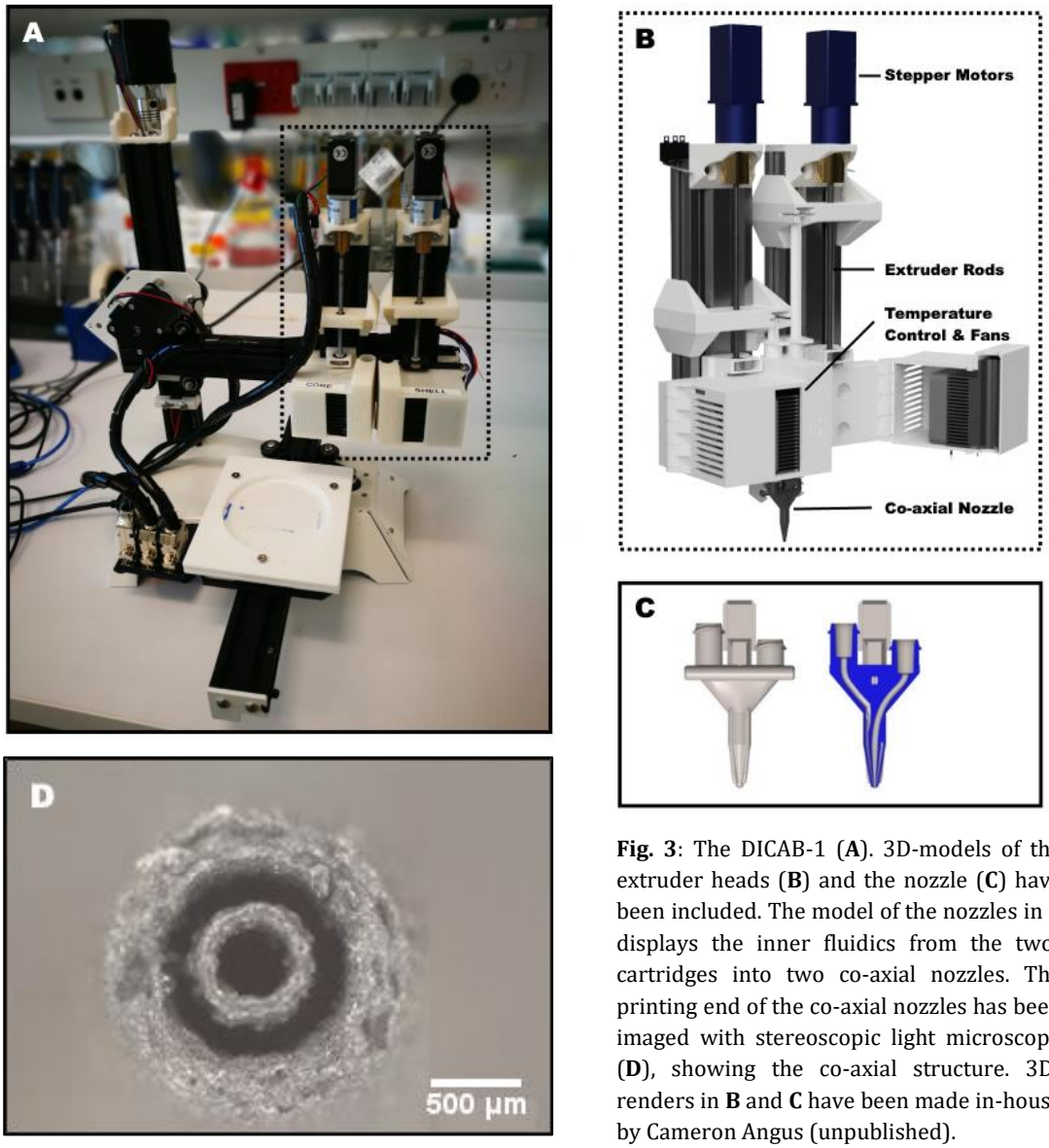

Fig. 3: The DICAB-1 (**A**). 3D-models of the extruder heads (**B**) and the nozzle (**C**) have been included. The model of the nozzles in **C** displays the inner fluidics from the two-cartridges into two co-axial nozzles. The printing end of the co-axial nozzles has been imaged with stereoscopic light microscopy (**D**), showing the co-axial structure. 3D-renders in **B** and **C** have been made in-house by Cameron Angus (unpublished).

3.2.2 Biomaterials

Two biomaterials were used for the fabrication of fibres and constructs with DICAB-1. Initially, the cartridges were loaded with 20% Pluronic F-127 as an inexpensive material for performing preliminary calibration, optimisation and characterisation of the set-up. Pluronic F-127, or Lutrol, is a triblock co-polymer (poloxamer 407) consisting of two blocks of poly-ethylene glycol surrounding a block of polypropylene glycol. It gels at temperatures above 4°C when dissolved in water. Below 4°C, it is an aqueous liquid.[96] Because of its reversable gelation, it is commonly used as a sacrificial or fugitive ink to allow for fabrication of complex structures.[97,98] Here, it is exclusively used as a material for preliminary experiments. Considering the cytotoxicity of Pluronic F-127[96], different materials that are biologically and clinically more relevant have been used for encapsulating and printing cells.

These experiments have been performed with a hybrid GelMA (gelatine methacryloyl)/alginate hydrogel. Both GelMA and alginate have been used extensively in tissue engineering and Biofabrication.[79,99,100] Both are non-cytotoxic and biocompatible. When dissolved, they form a viscous liquid that can be crosslinked into a hydrogel. Alginate has been used extensively in the past in islet encapsulation strategies as described above, and it is a favourable material because of its straightforward crosslinking mechanism and favourable mechanical properties. Nonetheless, as it is a polysaccharide it does not offer cell attachment moieties and as thus it needs to be chemically modified in order to mimic the natural ECM.[101,102] Contrarily, GelMA naturally offers abundant cell attachment moieties as it is derived from collagen, one of the major constituents of the ECM. GelMA is prepared through methacrylation of gelatine (a collagen derivative), which makes it photo-crosslinkable in presence of a photo-initiator.[103] By combining GelMA and alginate, a bioink can be designed that has favourable mechanical properties along with a cell-friendly ECM-like environment.

This hybrid hydrogel containing both GelMA and alginate had been previously defined, characterised and optimised for this project.[104] The bioink consisted of 7.5% GelMA and 2% alginate. The rheology of the bioink had been studied and predicted to be most suitable for printing at a temperature of approximately 15°C. This is also the prime reason why the temperature regulation in the DICAB-1 is essential. A final benefit of the use of this hybrid bioink had also been hypothesised in these previous studies. It was expected that the positive charge of GelMA may interact with the negative charge of the alginate, which may result in microphase separation and the formation of some micro-porosity.

3.2.3 Cells

Both endothelial cells and β-cells have been encapsulated in the bioink and incorporated in the constructs. Initially, fabricated constructs contained cells in single cell suspension derived from two cell lines: Mile Sven 1 (MS1) endothelial cells and β-TC-6 cells. Although cell lines are less suitable for translation to the clinic in the long-term, they posed a more cost-effective model system for some of the preliminary experiments compared to primary tissues or cells. The β-cell line, β-TC-6, has been used widely in the literature[104–107] and is well understood. As their biological function in for example GSIS is not optimal, however, these cells have exclusively been used to validate cell survival during printing and culture. Additional experiments have been conducted to investigate clinical relevance and GSIS experiments were conducted with printed mouse islets (at the University of Adelaide), which are far superior to any cell line in terms of GSIS. These islets were supported by isolated endothelial progenitor cells (EPCs), which are also a more clinically relevant model than the MS1 cells.

There are several reasons why both endothelial cells and islets have been incorporated into the constructs. One reason is that this allows for a proof-of-concept of co-delivery of two different cell types in co-axial fibres and demonstrates whether both endothelial as well as β-cells survive the printing and crosslinking process. More importantly, endothelial cells and in particular EPCs have previously been shown to have several beneficial effects on islet performance. The most obvious added value of EPCs is related to their potential for the development of vascularisation in the construct, which is primarily important for islet survival in the longer term through nutrient and oxygen delivery. Additionally, in future transplantation, this vascularisation will be essential to allow for the detection of host blood glucose levels and the transport of insulin. The presence of EPCs and their potential vascularisation have also been shown to improve engraftment upon transplantation.[108–110] Finally, EPCs may positively affect insulin gene transcription and secretion directly.[110,111]

3.2.4 Construct design

Initially, core/shell-fibres were printed with Pluronic and GelMA/alginate bioink to optimise printer performance. However, the final design consisted of bioprinted tissue constructs. Co-axial fibres of the GelMA/Alginate bioink were in the x/y-plane and stacked in the z-direction (**Fig. 4B**). The bioink in the core contained the functional cells (β-TC-6 or pancreatic islets). The bioink in the shell incorporated supporting, endothelial cells, to demonstrate co-deposition of two different cell types (**Fig. 4A**). After printing, constructs were dual-crosslinked. First, the GelMA network was crosslinked with visible light. Second, the alginate network was ionically crosslinked in a $CaCl_2$-bath. A more detailed description of the fabrication process is offered in the Methods section. Constructs incorporating primary mouse islets and EPCs consisted of a single-layer x/y-grid to limit size considering the limited availability of primary islets and ethical constraints.

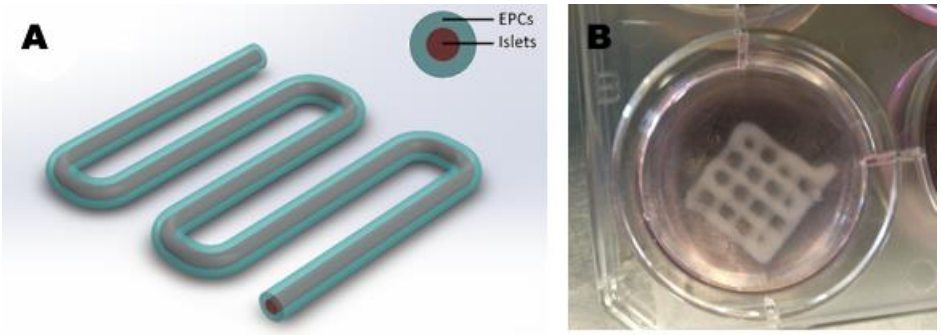

Fig. 4: The final construct design. The functional cells (islets or β-cells) are incorporated in the core-fibre, whereas the supporting endothelial cells are printed in the shell fibre, schematically represented in **A**. The constructs are deposited in an x/y-grid as exemplified in **B**.

Chapter 4

4. Methods

4.1 Preparation of materials

4.1.1 Preparation of Pluronic ink

Pluronic F-127 (Sigma-Aldrich) was suspended into deionised water (20% w/v) at 5°C. Full dissolution of Pluronic was allowed to occur overnight at 5°C. Before printing, Pluronic was dyed with common food colouring (red or blue) by mixing a small droplet of colouring into 50 mL stocks. Dyed Pluronic solutions were stored at 5°C until further use.

4.1.2 Bioink material synthesis and labelling and bioink preparation

Gelatine methacryloyl (GelMA) was prepared as described previously.[103] Briefly, gelatine of medium molecular weight (porcine skin, Type A, 175 Bloom, Sigma-Aldrich; 10% w/v) was dissolved overnight in phosphate buffered saline (PBS) at 37°C. Next, GelMA was synthesised by direct reaction with methacrylic anhydride (Sigma-Aldrich) at 50°C for 4 hours. To end the reaction, the solution was diluted with PBS and neutralised to pH 7.4, after which the solution was dialysed for two weeks and consecutively freeze-dried. Freeze-dried GelMA was stored at -20°C until further use. For fluorescent bioink, GelMA was labelled with rhodamine-B iso-thiocyanate (Sigma-Aldrich): a red fluorescent label that covalently attaches to proteins. Labelling was performed by dissolving a small amount of dye (1% w/v) in DMSO. This solution was added to GelMA dissolved in PBS (5% w/v) and the reaction was allowed to proceed for 4 hours at room temperature (RT) shielded from light. Labelled GelMA was freeze-dried after two weeks of dialysis. All dialyses were performed in deionised water at RT which was refreshed twice per day. The above procedures were performed under sterile conditions.

For the preparation of hybrid GelMA/alginate bioink, sodium alginate from brown algae (medium viscosity, Sigma-Aldrich; 2% w/v) was sterilised with UV-radiation for 20 minutes. Next, it was dissolved into sterile PBS at 37°C overnight with added 1% v/v streptomycin/penicillin (pen/strep; Life Technologies) and photo-initiator (LAP; lithium phenyl-2,4,6-trimethyl-benzoyl-phosphinate; 0.06%; Sigma-Aldrich (Wollongong) / TCI (Adelaide)). Sodium alginate solution was stored at 4°C until further use. Upon requirement of bioink, alginate solution was heated to 37°C and GelMA was stepwise added in small amounts to finally add up to a total concentration of 7.5% and dissolved by vigorous vortexing. The bioink was stored overnight at 37°C before use on the next day, to ensure complete dissolution of GelMA and mixing of the alginate and GelMA polymer networks.

For cell or islet encapsulation and printing experiments, initial bioink concentrations were adjusted to allow re-suspension of cells in medium into the bioink. 1.25× Concentrated bioink was similarly prepared as described above. Adjusted bioink concentrations were chosen (2.5% Alginate; 9.375% GelMA) to allow for suspension of concentrated cells or islets with medium in a 1:4 (medium : bioink) ratio.

4.2 2D-Cell culture

MS1 cells were cultured in Dulbecco's Modified Eagle Medium (DMEM; Life Technologies) further supplemented with 5% v/v foetal bovine serum (FBS), 1% v/v pen/strep (Life Technologies) and 1% v/v Glutamax (Life Technologies) under standard cell culture conditions (37°C, 5% CO_2). Cells were passaged at 90% confluency and entered the experiment at passage 10. Beta-TC-6 (β-TC-6) cells were similarly cultured in DMEM supplemented with 15% v/v FBS and 1% v/v pen/strep. MS1 cells were passaged 1:20, whereas β-TC-6 cells were passaged 1:3. β-TC-6 cells entered the experiment at passage 40 or 41 (from a previously established stock at passage 38).

4.3 Life/dead staining

For all non-primary cell printing and encapsulation, calcein AM/PI staining (calcein acetoxymethyl ester/propidium iodide; Sigma-Aldrich) was used. Constructs were taken from culture and washed with PBS. Next, constructs were incubated in 500 µL calcein AM (5 µM in PBS) for 15 minutes at 37°C, 5% CO_2. A small amount of PI (final concentration 1 µg/mL) was added to the solution and culture was continued for 5 more minutes in the same conditions. Staining solution was replaced with PBS and constructs were imaged with fluorescence microscopy (Zeiss Axiovert CF40). For islet printing experiments, FDA/PI (fluorescein diacetate/propidium iodide; Sigma-Aldrich) staining was performed instead. Constructs or free islets were washed with PBS and consecutively placed in 1 mM FDA and 5 µg/mL PI dissolved in PBS. Samples were incubated for 10 minutes and washed again with PBS. Images were recorded through confocal (Olympus FV3000) or fluorescence microscopy (Olympus CKX41) within an hour.

4.4 Cell proliferation/metabolism

To keep track of total cell metabolism as a measure of both proliferation and cell function, PrestoBlue assays were performed. Briefly, constructs were washed in PBS and placed into wells containing 1 mL standard culture medium supplemented with 1% PrestoBlue (ThermoFisher Scientific) and incubated for 4 hours (37°C, 5% CO_2). Supernatants were collected and fluorescence of supernatants was recorded at 544/590 nm in duplicates (BMG Labtech FLUOstar Omega). Constructs were washed in PBS twice before return to culture at intermediate time points.

4.5 MS1 cell encapsulation

MS1 cells were trypsinised from 2D-culture and suspended in medium containing 0.06% LAP and 10 ng/mL recombinant mouse VEGF. Cell suspensions were re-suspended into bioink containing 0.06% w/v LAP and 1% v/v pen/strep at approximately 2 million cells mL^{-1}. Cells suspended in bioink were cast into cylindrical custom moulds (5 mm diameter, 2 mm height). Consecutively, constructs were crosslinked first in visible light at 405 nm wavelength (Omnicure, BVL-4.LC, output 15%) for 60 seconds. Second, ionic crosslinking of the alginate network occurred in $CaCl_2$-baths (2% w/v; $CaCl_2$-dihydrate extra pure, Scharlau) for 10 minutes. Constructs were then cultured for three weeks in MS1

culture medium further supplemented with VEGF (10 ng/mL; Gibco). Cell viability (live/dead) and metabolism (PrestoBlue) was investigated at t = 0, t = 7, t = 14 and t = 21 days.

4.6 Printing of co-axial fibres with Pluronic and (labelled) bioink

4.6.1 Printer optimisation with Pluronic

All prints were performed onto standard microscope slides. Initially, the build plate distance was optimised by performing sweeps of different distances ranging from 0.7 to 1.3 mm at a feed rate of 400 mm/min and extrusion rate of 0.1 (-) with a core/shell-ratio of 1:1. Extrusion rate was defined as the distance (in mm) the extruding piston moved down per distance moved by the printhead (in mm). Build plate distance was optimised for fibre continuity, minimal variability in diameter and subjective print quality (i.e. to which degree the print matches the path of the G-code) to 0.9 mm, calibrated by lowering the nozzle to contact with the build plate before each print. Extrusion rates were consecutively optimised to 0.06 (-) for minimal variability in diameter by performing a sweep of extrusion rates (**Fig**. **S1**). Extrusion rates below 0.06 (-) led to recurring intermittent fibre printing due insufficient material deposition. The following, optimised parameters were used in all consecutive prints: 400 mm/min feed rate, 0.9 mm build plate distance and 0.06 (-) extrusion rate. All prints with Pluronic were performed with temperature system set to 12°C to decrease viscosity during printing, although actual cartridge temperature could not be measured and is expected to be higher due to single-sided contact with temperature regulation units.

4.6.2 Fabrication of co-axial fibres with Pluronic

Print G-codes were manually coded without additional CAD or slicing software. Codes have been provided in the appendix (**Appendix B**). Prints were performed at core : shell extrusion ratios of 4 : 96 and 16 : 84. Pluronic labelled with blue and red food dye was extruded through core and shell, respectively. Pictures were recorded with stereoscopic microscopy (Leica M205A) and core and shell fibre diameters were measured in ImageJ software from two independent prints performed on different days in triplicate.

4.6.3 Fabrication of GelMA/alginate co-axial fibres

For printing GelMA/alginate bioink, different parameters needed to be established for reliable extrusion. Parameters for printing core/shell-fibres with a diameter ratio of approximately 1:1 were optimised through trial and error to an extrusion rate of 0.010 (-) at a feed rate of 400 mm/min with system temperatures set to 15°C onto glass slides pre-cooled to 5°C at a distance of 0.7 mm. Due to time constraints, material cost and labour intensity of material synthesis, no complete parameter optimisation sweeps were performed with bioink. Fluorescently labelled bioink (5% labelled GelMA of total GelMA content) in the core was co-printed with unlabelled bioink in the shell and consecutively photo- and ionically crosslinked as described above. Images were recorded directly after printing through fluorescence microscopy (Zeiss Axiovert CF40).

4.7 2D MS1 and β-TC-6 metabolism and proliferation assays

MS1 and β-TC-6 cells were cultured in β-TC-6 culture medium in T75 flasks in triplicates. At t = 0, 1.6 million cells were seeded. Cell counts were performed at t = 0, t = 1 and t =3 days because of the high proliferative rate of MS1 cells (Invitrogen Countess 1754B). At the same time points, total metabolic rates were established with PrestoBlue assays as described above prior to cell counts.

4.8 Bioprinting MS1 and β-TC-6 cells

β-TC-6 and MS1 cells were expanded to sufficient cell numbers in 2D-cell culture flasks and encapsulated in bioink as described above. β-TC-6 cells were encapsulated at approximately 6 million cells mL^{-1}, whereas MS1 cells were encapsulated at approximately 1 million cells mL^{-1}. Co-axial fibres were printed at an extrusion rate of 0.010 (-) with a feed rate of 400 mm/min with system temperature settings at 15°C onto pre-cooled glass slides (5°C). Cell viability was established at t = 1 and t =7 days post printing as described above.

For attempted CD31 labelling, small parts of fibres were excised from prints and fixed with 3.7% PFA (paraformaldehyde) for 20 minutes at RT. Samples were washed with PBS and incubated for 1 hr at RT in 1% BSA (bovine serum albumin) in PBS. Fibres incubated with directly conjugated anti-mouse CD31/FITC monoclonal antibody (ThermoFisher, 11-0311-82) for 1 hr or 24 hrs in 1:20 and 1:50 dilutions (in different attempts). Samples were washed again and stained with DAPI for 5 minutes prior to imaging with fluorescence microscopy.

4.9 Fabrication of 3D-constructs with bioink

6-layered constructs of approximately 1.5 × 1.5 × 0.5 cm were fabricated at previously mentioned parameters for GelMA/alginate bioink. Trace fluorescently labelled GelMA (5% of total GelMA content) was incorporated in the core, whereas shell fibres were unlabelled. During deposition of each layer, bioink was crosslinked for 40 seconds with visible light (Omnicure, BVL-4.LC, output 15%). After deposition of the first two layers, partial ionic crosslinking was achieved by dropping small volumes (40 µL total) of $CaCl_2$-solution (2% w/v) evenly onto the printed bioink. Ionic crosslinking was completed after all layers were deposited by submerging constructs in 2% $CaCl_2$-baths for 10 minutes. Images were recorded through stereoscopic microscopy (Leica M205A).

4.10 Murine EPC and islet isolation and culture*

4.10.1 Isolation and culture of murine islets

Mice (C57BL/6) were euthanised according to all ethical standards and guidelines. Pancreata were isolated and perfused with 3 mL cold collagenase solution. Samples were allowed to reach 37°C and

* Murine EPC and islet isolation was performed by Daniella Penko at the University of Adelaide

30 mL of islet wash medium (M199; Gibco) was added. Samples were shaken hard and vortexed, before being spun down at 300G for 3 minutes. Supernatants were decanted; this wash procedure was repeated. Degraded pancreata were then sieved twice. Islets were then separated using Lymphoprep (Stemcell Technologies) and finally washed several times using islet wash medium. Islets were cultured for one day in complete islet medium (RPMI 1640; Gibco; supplemented with 10% FBS and 1% pen/strep (v/v)) and counted under light microscopy (Olympus CKX41) before printing.

4.10.2 Isolation and culture of murine EPCs

Mice (C57BL/6) were euthanised according to all ethical standards and guidelines. Femurs and tibia were isolated and separated from muscle and tendons. Ends of tibia and femurs were cut off and bone marrow was flushed out with 37°C EPC wash medium (HUVE supplemented with 20% FBS; Gibco) applied through a 23G needle. Bone marrow was broken down and blended into single cell suspension through pipetting up and down through EPC wash medium. T25 cell culture flasks were coated with fibronectin (500 µL per flask at 50 µg/mL; Roche). Cells were counted and transferred to fibronectin-coated T25 flasks. Cells were allowed to adhere for 1 day in EPC culture medium (HUVE with 20% FBS, further supplemented with heparin (0.045 µg/mL; BD Bioscience) and endothelial growth factor (0.045 µg/mL; BD Bioscience); 37°C, 5% CO_2). Non-adherent cells were removed and EPCs were cultured in EPC-medium for 6 days before printing.

4.11 Islet/EPC-construct fabrication and culture

DICAB-1 was sterilised with 70% ethanol and moved into a PC2 Biosafety Cabinet. Nozzles, cartridges, petri-dishes, tweezers and needle tips were sterilised with 70% ethanol which was allowed to evaporate for 30 minutes. Islets or EPCs were collected and counted as described above and re-suspended in LAP-supplemented (0.06% v/v) islet medium at 2500 islets mL^{-1} or 12.5 million cells mL^{-1}. Next, resuspended islets or EPCs were encapsulated into 1.25× concentrated bioink (pre-warmed to 37°C), resulting in a final 1× concentration of bioink (7.5% GelMA / 2.0% alginate) with 500 islets mL^{-1} or 2.5 million EPCs mL^{-1}. Bioink with suspended islets or EPCs was loaded into core or shell cartridges, respectively, and consecutively pre-cooled on ice for 5 minutes to ensure increased viscosity and printability. Constructs consisted of single-layer x/y-grids of 2 cm by 2 cm with 0.5 cm fibre spacing. Constructs were photo-crosslinked during printing for 40 seconds at 10% intensity (OmniCure LX505) at an approximate distance of 1.0 cm, followed by 40 seconds photo-crosslinking post-printing. Constructs were consecutively ionically crosslinked in 2% $CaCl_2$-baths (BDH AlanaR) for 10 minutes, before transfer to non-adherent 6-well plates for culture in 2 mL complete islet medium. Constructs and free-floating islets were investigated at t = 1 and t = 3 days post-printing.

4.12 Glucose Stimulated Insulin Secretion

Constructs containing islets (core) and EPCs (shell), constructs containing islets only, negative

controls (constructs without islets or EPCs) and free-floating islets were carefully collected from culture and placed in Eppendorf cups. Constructs were washed with Krebs buffer supplemented with 2 mM glucose and consecutively allowed to recover with the same buffer for 30 minutes. Next, constructs or free islets were incubated for one hour with open lids (37°C; 5% CO_2) in Krebs buffer containing 2 mM and consecutively 20 mM glucose. After both incubations, supernatants were collected for further investigation.

Supernatants were then used in an insulin-detecting ELISA (Mercodia), following the manufacturer's instructions. Briefly, small volumes of supernatants were pipetted into 96-well plates coated with monoclonal anti-insulin (murine) in duplicates. Peroxidase-conjugated monoclonal anti-insulin was added and samples were incubated for 2 hours at RT. Wells were washed several times and substrate (3,3',5,5'-tetramethylbenzidine) was added to each well; reactions were allowed to proceed at RT for 15 minutes before being halted with 0.5M H_2SO_4. Optical density of the wells was then read within 30 minutes at 450 nm (Bio-Rad Model 680). Negative controls were subtracted as blanks for constructs, whereas regular blanks were subtracted from free-floating islets. Standard curves based on manufacturer's calibrator samples were used to calculate results (see statistical analyses below); a 1:10 dilution was included for the 20 mM glucose samples in order to ensure results were within reliable detection range.

4.13 Hypoxia in scaffolds

Single-layer scaffolds of 2.0 by 2.0 cm (i.e. the same scaffold design used for printing islets and EPCs) were fabricated as described previously. For these experiments, EPCs were incorporated into both shell and core fibres of the scaffold. At one day post-printing, scaffolds were cultured at normoxic conditions for 4 hours at 37°C (5% CO_2) in islet culture medium supplemented with a hypoxia reagent (Invitrogen Image-iT green hypoxia reagent) at 1 µL/mL. Scaffolds were then cut into smaller samples (0.5 by 0.5 cm) to allow for imaging with confocal microscopy (Olympus FV3000). Hypoxic and normoxic controls were established by plating EPCs in 6-well plates in the same medium for 4 hours in 1% O_2 or normal oxygen concentrations, respectively. Cells were then trypsinised and similarly imaged through confocal microscopy.

For quantifiable data, flow cytometry (BD FACSCanto II) was used. Scaffolds and controls were cultured for 4 hours in conditions described above, in medium supplemented with 0.2 µL/mL hypoxia reagent. Scaffolds were then digested using a mixture of enzymes (Gibco TrypLE Express) with intermittent vortexing and pipetting up and down until full degradation. Hypoxic and normoxic controls were trypsinised and data were obtained through flow cytometry in triplicates and analysed with FCS Express 6 Flow Cytometry Software.

4.14 Statistical analyses

All statistical analyses have been performed in standard IBM SPSS software. Where relevant, data are shown with the 95% CI (confidence interval) or the standard deviation. Unless otherwise stated, tests for significantly different means were performed with one-way ANOVAs with Bonferroni post-hoc

tests. In a few cases (explicitly stated in figure legends), the ANOVA assumption of homogeneity of variance was not met (established through Levene's test for homogeneity of variances) and Welch's test was used instead.

For the analysis of the GSIS, a standard curve was plotted based on reagents from the manufacturer. A cubic spline regression was employed to plot the curve, from which the unknown concentrations were interpolated in duplicates. Two independent experiments were performed with a sample size of three, leading to a total N = 6. Duplicates were averaged and data are represented with 95% CI of the mean of N = 6.

Chapter 5

5. Results

5.1 Proof-of-concept printing of co-axial fibres

First, the properties of the printer were evaluated and it was investigated whether and how co-axial fibres could be fabricated reliably. Initially, 20% Pluronic F-127 (Lutrol) was used, before moving to the less readily available, more labour-intensive and costlier bioink.

5.1.1 Pluronic F-127

As an initial test, Pluronic was printed through both core and shell nozzles. In order to visualise the core/shell-structure in the co-axial fibres, the Pluronic in the core and shell cartridge were coloured with blue and red food dye, respectively. Two examples of the resulting core/shell-fibres with varying core diameters are displayed below in **Fig. 5**.

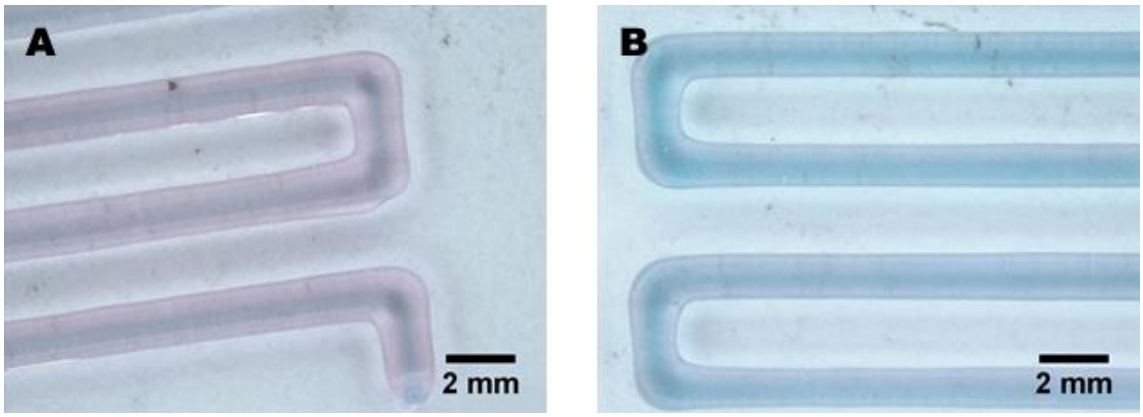

Fig. 5: Co-axial fibres printed with the DICAB-1 with two different core and fibre diameters. Pluronic F-127 was extruded through both core and shell nozzles at two different ratios (4:96 in **A** and 16:84 in **B**) to achieve different core diameters. Pluronic F-127 was dyed with a blue food colouring dye or a red food colouring dye to visualise core and shell fibres, respectively.

Using an extrusion ratio of 4 : 96 (core : shell), it was established that it was possible to fabricate fibres of a total diameter of 1.45 ± 0.044 mm and a core diameter of 0.46 ± 0.091 mm, represented in **Fig. 5A**. Varrying this extrusion ratio, but not the total extrusion rate, was found to affect the core/shell-diameter ratio, but also to a smaller degree the total (outer) diameter. Extruding at a ratio of 16 : 84 (core : shell) was found to result in fibres with a total diameter of 1.27 ± 0.092 mm and a core diamter of 0.67 ± 0.087 mm (**Fig. 5B**). As such, it had been confirmed that the platform is capable of producing core/shell-fibres with reasonable control over fibre diameters and core/shell-ratios. Next, the parameters were further optimised to constrain total fibre diameter to within 1 mm (**Fig. S1**). Given the limited clinical relevance of Pluronic due to its cytotoxicity[96], however, no further

experiments were conducted relying on this material and it was next evaluated whether fabrication of co-axial fibres was feasible with the GelMA/Alginate-bioink.

5.1.2 Fabricating co-axial fibres with GelMA/alginate Bioink

Thus, as a next step, the GelMA/alginate bioink was used to fabricate co-axial fibres. This was first demonstrated in a cell-free proof of concept. To still visualise a core/shell-structure in the fibres, a fluorescently labelled GelMA was synthesised. Before bioink preparation, GelMA was covalently labelled with rhodamine-B-isothiocyanate. A small portion of this labelled GelMA (5% of total GelMA content) was blended into the bioink. The resulting labelled bioink was loaded into the cartridge for the extrusion of the core fibres. The concentration of unlabelled GelMA in the core was slightly adjusted to make sure the total GelMA concentration remained consistent at 7.5% between core and shell fibres. The shell cartridge for these prints was loaded with unaltered 7.5%/2% GelMA/alginate bioink.

Fibres were printed and consecutively photo-crosslinked with visible light and ionically crosslinked in 2% $CaCl_2$ baths. Immediately after printing, fibres were analysed with fluorescence microscopy (**Fig. 6B**). The fluorescent channel was superimposed (**Fig. 6C**) with a brightfield image (**Fig. 6A**) in order to clearly visualise the whole fibre. In these images, only the centre of the fibres shows fluorescence. The fluorescently labelled GelMA is therefore contained within the core of the fibres, indicating successful fabrication of co-axial fibres. Some red can be observed outside the border of the printed co-axial fibres, but this is attributed to reflection of fluorescence on the glass microscope plate surface.

Two additional observations can be made from the imaged fibres. First, even in the brightfield image (**Fig. 6A**), a core/shell-structure seems observable that matches the structure observable in the fluorescent channel. This is somewhat unexpected, since apart from a trace amount of labelled bioink, the material of core and shell are identical. A more continuous and monolithic appearance of the fibre in the brightfield channel was therefore expected. It is unsure whether these borders are an effect of the extrusion through a co-axial nozzle or a small difference in material properties due to the presence of labelled GelMA. The direct area surrounding the core fibres also shows some mild fluorescence that decreases with distance. This may indicate some limited diffusion of labelled GelMA into part of the shell fibres prior to fibre crosslinking. Nonetheless, a clear shell without any fluorescence is still observable, indicating successful fabrication of co-axial fibres.

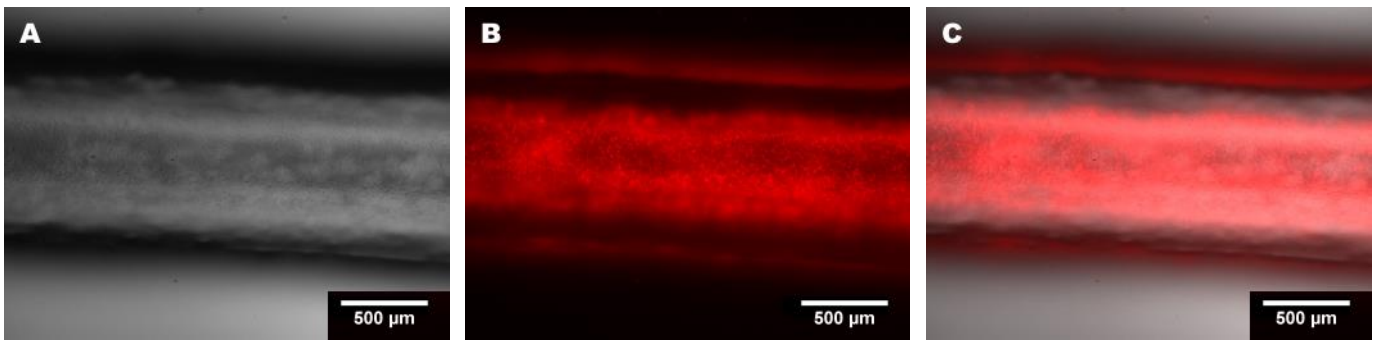

Fig. 6: Co-axial fibres of GelMA/alginate bioink printed with DICAB-1. Images of brightfield (**A**), fluorescent channel (**B**) and a superposition of both channels (**C**) have been displayed of an extruded fibre with GelMA/alginate bioink with trace (5% of total GelMA content) fluorescently labelled GelMA in the core.

5.1.3 Fabrication of 3D-constructs with GelMA/alginate bioink

Since of printing core/shell-fibres with the platform had been confirmed, it was next investigated whether it was feasible to fabricate 3-dimensional constructs with stacked fibres in the z-direction. To this end, labelled (core) and unlabelled bioink (shell) was printed into co-axial fibres which were deposited in an x/y-grid in layers. During printing of each layer, bioink was crosslinked with visible light. Six layers were printed resulting in constructs with a height of approximately 0.5 cm.

In initial prints, it was found that in spite of the current temperature control set-up, cooling was not effective enough to increase viscosity for reliable fibre stacking. It was decided to pre-cool the glass collection slides to 5°C to maintain lower temperatures after deposition and during crosslinking. Additionally, partial ionic crosslinking was allowed to occur by dropping small volumes of $CaCl_2$-solution onto the first two layers after printing of each layer. This also led to partial crosslinking of the additional layers upon deposition, increasing shape fidelity despite lower viscosities.

With these additional measures, 6-layered constructs could be printed with reasonable control (**Fig. 7**). Although most porosity could be maintained, pore size was not consistent within the constructs, with decreased pore size around the borders. Occasionally, pores were still completely blocked in corners as exemplified in **Fig. 7**. These limits in print quality were attributed to sub-optimal cooling as fibres were still somewhat liquid upon deposition, leading to 'leaking' into pores upon stacking of additional layers. This sub-optimal cooling was confirmed as temperature regulation units were unable to reach target temperatures at the interface with the cartridge, which suggests bioink temperatures were higher still within the cartridges. In future improved iterations

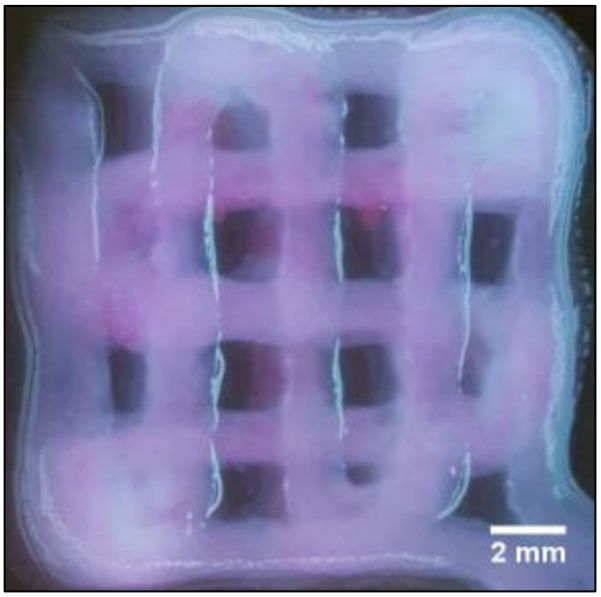

Fig. 7: Top-view of a 6-layered construct with labelled bioink (pink, core) and unlabelled bioink (colourless). Print quality was significantly inferior compared to single fibres, in spite of additional measures to improve print quality. Porosity can be observed to be maintained but inconsistent and core/shell-structure was less apparent. Image recorded through stereoscopic microscopy.

of DICAB-1, temperature control will be enhanced and it is expected that improved print quality with fibre stacking should be feasible at that stage.

Most labelled bioink filaments, which appear pink in light microscopy, were localised towards the core of the fibres. However, in line with insufficient viscosity for layer stacking, the prolonged printing time before crosslinking led to increased blending between core and shell fibres, with core/shell-structure less apparent than in single fibres (**Fig. 5** and **Fig. 6**). Additionally, minor shifts in position between stacked fibres may lead to less apparent localisation of labelled bioink in core fibres in a top-view.

Based on these observations, it was established that the current generation of DICAB-1 only possessed limited capability for the reliable fabrication of multi-layered constructs despite additional measures for shape fidelity such as pre-cooled collection slides and moderate ionic and photo-crosslinking during printing. Before larger multi-layered constructs can be fabricated with consistent porosity and more reliable core/shell-structure, improved cooling will be a primary necessity.

5.2 Encapsulation of MS1 cells

It was investigated whether the encapsulation and crosslinking processes by themselves, irrespective of printing, were cell-friendly and whether the 7.5%/2% GelMA/alginate-bioink could sustain a long-term 3D-cell culture. To this end, a mouse endothelial cell line (Mile Sven-1; MS1) was first grown to sufficient cell numbers in traditional 2D-cell culture flasks and consecutively encapsulated in bioink. Cells encapsulated in bioink were then mould-casted into custom cylinders (5 mm diameter, 1 mm height). The bioink was then photo-crosslinked and ionically crosslinked as described previously. The resulting constructs were cultured for three weeks in presence of 10 ng/ml recombinant mouse VEGF (vascular endothelial growth factor) supplemented in the culture medium.

VEGF is a growth factor which enhances the development of vascularisation through angiogenesis. It was chosen as a suitable supplement as it has been used in the past to stimulate vascularisation in the context of encapsulated islets[112] and it furthermore plays a major role in the vascularisation of islets *in vivo*, where it is secreted by pancreatic endocrine cells[78].

In order to evaluate cell viability after encapsulation and crosslinking, live-dead staining was performed at 1 day after encapsulation (**Fig. 8A**). Additionally, viability was evaluated after 21 days to investigate whether the GelMA/alginate hydrogel could sustain long-term culture (**Fig. 8B**). At day 1, it can be seen that cells are predominantly present in single-cell suspension, which can be expected at such short time after trypsinisation from 2D-cell culture. Most cells stain green indicating good viability, although there are a few cell agglomerations that seem to have died. These may be a result of incomplete trypsinisation prior to encapsulation, and due to their increased size they may have been subjected to increased shear stress during mould casting. At 21 days, over-all cell viability is maintained and cells have proliferated substantially over time. In addition, cell spreading and some alignment can be observed as a sign of biological activity.

In order to further evaluate the cell-spreading and morphology over time, higher magnification images were also obtained at intermittent 7-day intervals. These have been depicted in **Fig. 9**. In particular, it was investigated whether, as a result of supplemented VEGF in the medium, MS1 cells formed an endothelial cell network. At t = 7 and t = 14 days, only limited local cell spreading was observed at higher magnifications (**Fig. 9A** and **9B**), which was slightly more substantial at 14 days as can be expected. At t = 21 days, cell spreading was more obvious and continuous throughout the construct (**Fig. 9C, 9D** and **9E**), which indicates biological activity is maintained during culture. The increasing cell density over time which was also observed in **Fig. 8A** and **Fig**. **8B** was also mirrored at these higher magnifications. In general, observed cell alignment and proliferation suggests sustained biological activity of MS1 cells over-time.

Although cell alignment was observed, no vascular structures or continuous endothelial cell network formation were observed. In the future, these experiments may be repeated to further investigate the development of vascularisation. Perhaps concentrations of added VEGF may still be optimised. Most importantly, the visualisation may be improved through the use of confocal microscopy in order to also investigate lumen formation of potential endothelial cell networks, which is an essential part of the development of functional vasculature.

As an additional measure of biological activity of the encapsulated MS1 cells, and to confirm proliferation, total cell metabolism was tracked over time at seven-day intervals (**Fig. 10**). In line with the observed proliferation in images displayed in **Fig. 8** and **Fig. 9**, the total metabolic rate of the encapsulated MS1 cells increased over time. During the first two weeks, proliferation resembles an exponential growth, which somewhat slows down or staves off after the second week. The decreased growth during the third week may be due to the hydrogel achieving a saturated population of MS1 cells, as the hydrogel in **Fig. 8B** does suggest a densely populated hydrogel at 3 weeks.

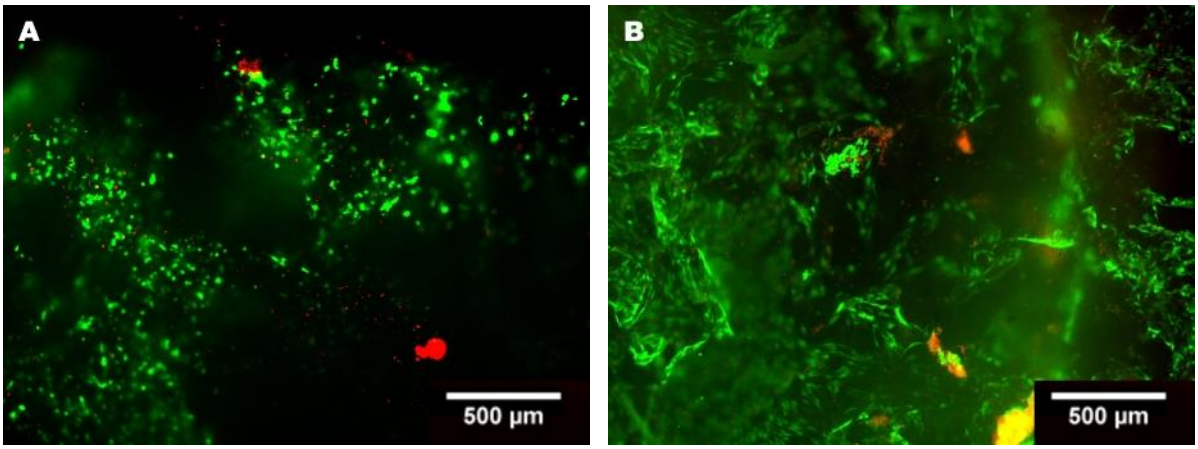

Fig. 8: Live/dead staining (calcein AM/PI) of encapsulated MS1 endothelial cells in GelMA/alginate bioink. Cells were encapsulated at 5 million mL^{-1} and consecutively cultured over the course of three weeks in MS1 medium in the presence of VEGF. Images have been recorded at t = 0 (**A**) and t = 21 (**B**) days through fluorescence microscopy.

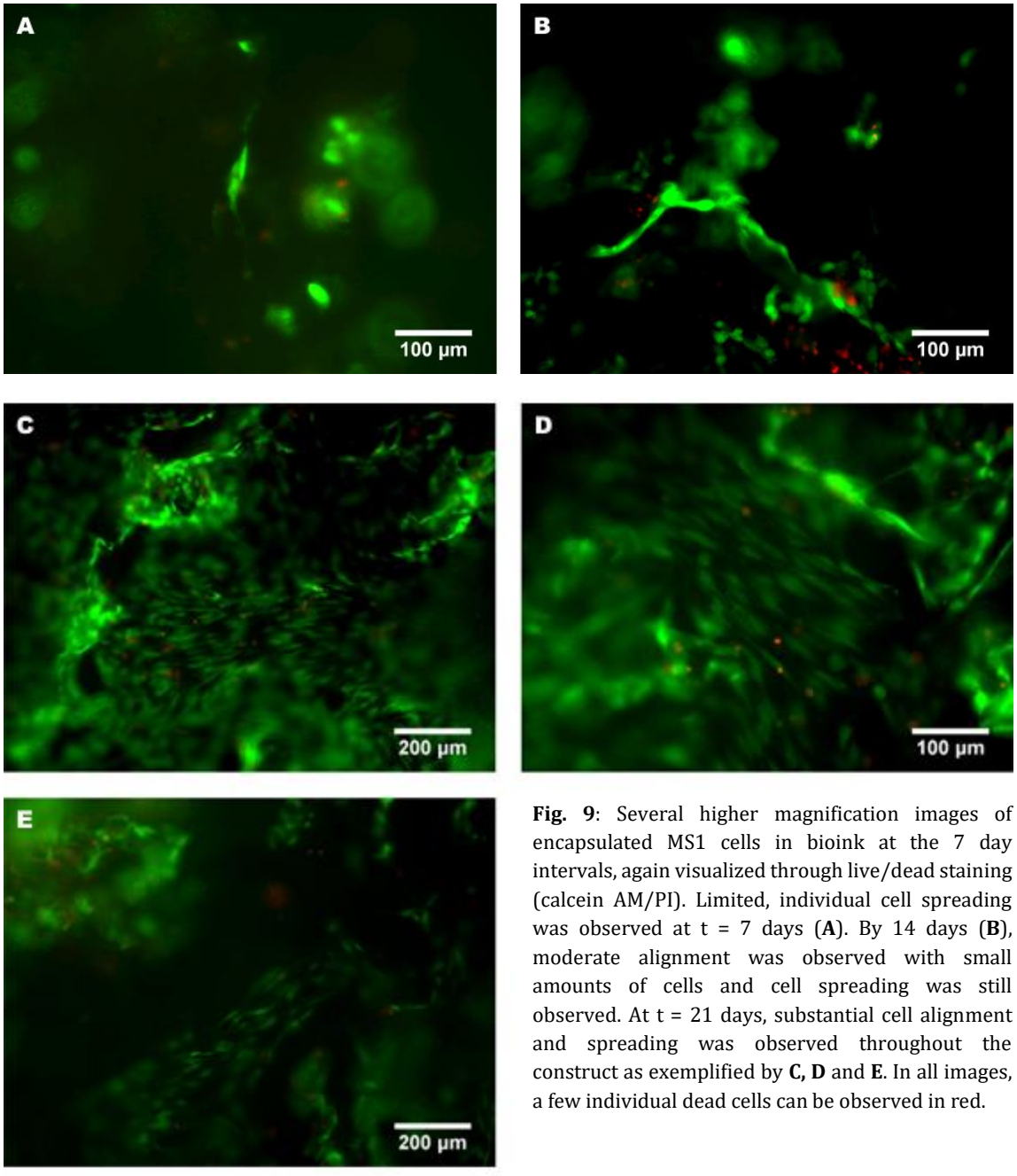

Fig. 9: Several higher magnification images of encapsulated MS1 cells in bioink at the 7 day intervals, again visualized through live/dead staining (calcein AM/PI). Limited, individual cell spreading was observed at t = 7 days (**A**). By 14 days (**B**), moderate alignment was observed with small amounts of cells and cell spreading was still observed. At t = 21 days, substantial cell alignment and spreading was observed throughout the construct as exemplified by **C, D** and **E**. In all images, a few individual dead cells can be observed in red.

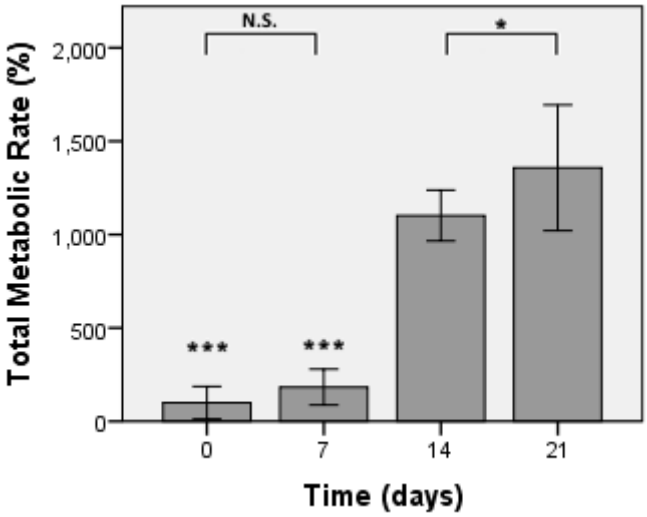

Fig. 10: Total metabolic rate of encapsulated MS1 cells in GelMA/alginate bioink. Cells were encapsulated at 5 million mL^{-1} and consecutively cultured over the course of three weeks in MS1 medium in the presence of VEGF. Total Metabolic Rate has been represented as relative to the mean rate at t = 0 days (100%). N = 3, error bars denote the 95% CI.

The combined results of the MS1 encapsulation in **Fig. 8, Fig. 9** and **Fig. 10** show that cells are viable both shortly after encapsulation and crosslinking, as well as after long term culture and remain metabolically and biologically active. These data suggest the crosslinking process is sufficiently cell-friendly and the platform can support cell culture over at least three weeks.

5.3 Establishing co-culture of MS1 and β-TC-6 cells

Since the printability of the GelMA/alginate bioink was shown and basic cell compatibility had been confirmed in encapsulation experiments, it was next established whether the present printing platform was cell-compatible. To this extent, two different cell lines were co-printed in core and shell fibres. Before these experiments could be conducted, however, it is necessary to design a feasible co-culture platform for the two cell-types.

There are some considerations to take into account before a co-culture can viably be established of two different cell types.[77] Firstly, a cell culture medium needs to be established that can support both cell types. As different cell types commonly have different standard culture media, this often results in a mismatch in optimal conditions for both cell types. In this platform, a β-cell line and an endothelial cell line were going to be co-cultured: β-TC-6 and MS1 cells, respectively. Considering that the biological function of the β-cells was clinically most relevant and important, it was first attempted to establish a co-culture relying on the optimised β-TC-6 culture medium. Thus, it was first investigated if β-TC-6 medium was able to support MS1 cell culture in traditional 2D-cell culture flasks. This was confirmed and there was no noticeable difference in MS1 morphology or behaviour across the different culture media in standard 2D-culture (data not shown).

A second consideration for the co-culture of two different cell types is their relative proliferative and metabolic rates. A considerable difference between cell types in either of these can result in overgrowth of one cell type or starvation due to outcompeting for nutrients, respectively. This would result in an unstable co-culture where only one cell type remains after some time in culture.

In order to obtain a quantified indication of the relative proliferative and metabolic rates of the two cell lines, a simple 2D-culture system was employed. Cells were cultured for 3 days and counted at day 1 and 3. In addition, their total metabolic rate was measured at the same time points (prior to counting).

The results have been depicted below in **Fig. 11**. Based on these data, it is apparent that MS1 cells far outperform β-TC-6 cells in terms of both proliferation and total metabolic rate. Over the course of three days, an exponential growth in cell number can be observed, whereas the β-TC-6 cell count remains stable. In line with this, the total metabolic rate of MS1 cells increases over time, whereas for β-TC-6 cells this even appears to decrease at three days.

Decreasing metabolic activity of β-TC-6 cells within three days is a troublesome sign for their biological function. However, it needs to be taken into consideration that in order to establish cell count, the samples were trypsinised and re-seeded at both one day and three days after the start of the experiments. It is possible that the substantial handling of the cells led to some decreased cell functionality and hence this may be not be a reliable indication of their metabolic rates if cells were left unhandled. MS1 cells may have been less affected by this handling due to their previously observed robust proliferative potential (**Fig. 8**, **9** and **10**). Also, it needs to be stressed that the suggested decline between β-TC-6 metabolic rate between t =1 and t = 3 days was not statistically significant, and is therefore inconclusive. The discrepancy in metabolism and proliferation between the two cell types is nonetheless clearly shown and too prominent to be ignored for future co-culture experiments. To compensate for this discrepancy, in the following experiments MS1 cells were encapsulated at significantly lower concentrations than β-TC-6 cells in a 3D(-printed) co-culture platform.

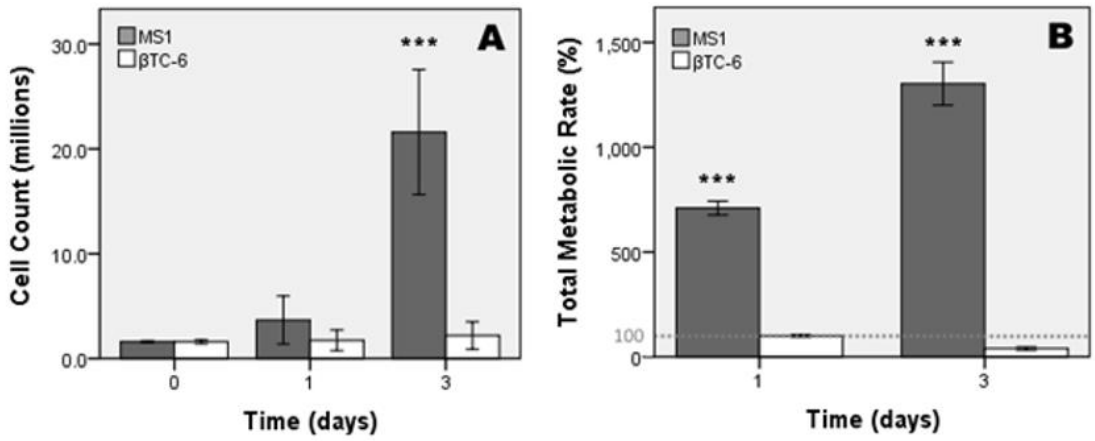

Fig. 11: Cell count (**A**) and total metabolic rate (**B**) of MS1 and β-TC-6 cells in traditional 2D-culture over the course of three days; 1.6 million cells were initially seeded at t = 0 days. Both cell types were cultured in medium optimised for β-TC-6 cells. Total metabolic rate has been calculated as relative to the metabolic rate of the β-TC-6 cells at t = 1 day (100%). N = 3, error bars denote the 95% confidence interval (CI). Significant differences were found through Welch's robust means test in **B**. *, ** and *** denote significant differences at the 0.05, 0.01 and 0.001 level, respectively.

5.4 Bioprinting co-axial fibres with MS1 and β-TC-6 cells

To evaluate whether the present platform was cell-friendly, encapsulated MS1 and β-TC-6 cells were co-printed into fibres in shell and core, respectively. Cell viability was evaluated through live/dead-staining at t = 1 and t = 7 days (**Fig. 12**). In order to compensate for the observed discrepancy in proliferation and total metabolic rate between MS1 and β-TC-6 cells, cells were encapsulated in a 1: 6 ratio (MS1 : β-TC-6).

Some cell death was expected, considering the shear stress, two crosslinking steps and substantial handling of the encapsulated cells during and prior to the printing process. At the day of the experiment, there were some additional technical difficulties with the customised DICAB-1 as the cooling malfunctioned. This turned out to be a slight design fault, which was resolved later on during experiments described below. During this experiment this led to cells being suspended in un-crosslinked bioink for 2-3 hrs more than intended. This was also expected to substantially affect viability. Nonetheless, cells were seen to survive the encapsulation, printing and crosslinking steps relatively well at one day post printing (**Fig. 12A**), although a moderate amount of individual dead cells was present as expected. Cells at this stage possessed spherical morphologies and were still present in single cell suspension. After seven days (**Fig. 12B**), cell spreading had occurred to some degree.

Since the shell fibre, which contained MS1 cells, fully encloses the core fibre with β-TC-6 cells, the different encapsulation concentrations of these two cell types cannot be observed in these images recorded through fluorescence microscopy. In order to confirm successful localisation of MS1 and β-TC-6 cells in shell and core, respectively, additional staining was performed with labelled anti-CD31 antibodies (an endothelial cell marker) counterstained with DAPI (a general cell nucleus marker) in

separate samples. However, no green fluorescence corresponding to CD31-positive cells could be observed, across various attempts. These results have been exemplified in the supplemental figures (**Fig. S2**).

CD31 makes up a substantial part of endothelial cell intercellular junctions. Hence, the lack of CD31-positive staining may either indicate: i) there are no MS1 cells present; ii)_the MS1 cells have not formed any cell junctions due to low cell density; iii) or MS1 cells have lost CD31-expression. As it was unlikely that no MS1 cells were present in the fibres, it is reasonable to rule out possibility i). Control experiments were performed with MS1 cells in basic 2D cell culture in which CD31 labelling was attempted. Here, too, no fluorescence was observed (data not shown). Given the substantial cell-cell contact in these 2D-culture experiments, it is unlikely that possibility ii) is the sole root-cause of failed staining. Thus, it was ultimately hypothesised that MS1 cells had lost CD31-expression, considering the relatively high passage number and tumoral origin of MS1 cells,.

In the future, this experiment may be repeated with a clinically and biologically more relevant cell line, such as EPCs used in experiments below. This would allow for more reliable CD31-expression to allow for visualisation of the localisation of endothelial cells. Optimally, this should be recorded through confocal microscopy. As at the time of the experiment such cells were not readily available, and due to the limited clinical relevance of MS1 cells, these experiments were ultimately discontinued and focus shifted towards experiments with clinically more relevant cells. Due to unsuccessful labelling of endothelial cells, it can also not be concluded whether MS1 cells or β-TC-6 cells, or both, showed cell spreading at t = 7 days (**Fig. 12B**). This is predominantly attributed to the MS1 cells, based on the limited activity of β-TC-6 cells shown previously and previously observed behaviour of MS1 cells (**Fig. 8** and **Fig. 9**).

Notwithstanding the above, sufficient cell viability at one and seven days after printing had been confirmed and therefore the present platform was deemed sufficiently cell-friendly in order to move towards clinically more relevant primary islets and endothelial cells in the next series of experiments.

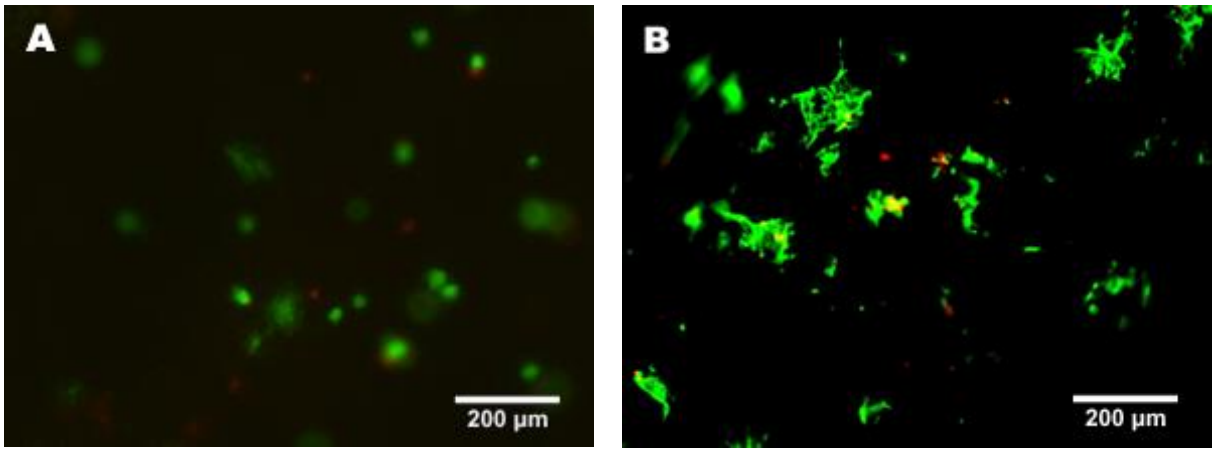

Fig. 12: Live/dead staining (calcein AM/PI) of co-printed MS1 and β-TC-6 cells in shell and core respectively, at t = 0 (**A**) and t = 7 (**B**) days. MS1 and β-TC-6 cells were encapsulated and printed in a 1 : 6 ratio and cultured in optimised β-TC-6 medium. Images recorded through fluorescence microscopy.

5.5 3D-printing of murine islets and EPCs

As a final series of experiments, it was evaluated whether the platform could also support cells that are more similar to those used in potential future animal trials and possibly clinical applications. Primary EPCs and islets were isolated from mice and encapsulated and printed following similar procedures as described above. Constructs of 2 by 2 cm were fabricated consisting of core/shell-fibres deposited in an x/y-grid (**Fig. 13**). Due to ethical considerations and material cost of primary cells, a limited number of islets and EPCs was available. Therefore, to limit construct size, only single-layered constructs were fabricated for these experiments. Constructs incorporated 500 islets mL^{-1} in the core fibres and 2.5 million EPCs mL^{-1} in shell fibres. Furthermore, considering the size of murine islets (up to 250 µm diameter), a wider nozzle (inner nozzle diameter: 502 ± 14 µm; outer nozzle diameter: 1241 ± 46) µm was employed for these prints compared to previous experiments to limit shear stress and risk of clogging. The use of this larger nozzle resulted in slightly larger fibres with a diameter of approximately 2 mm.

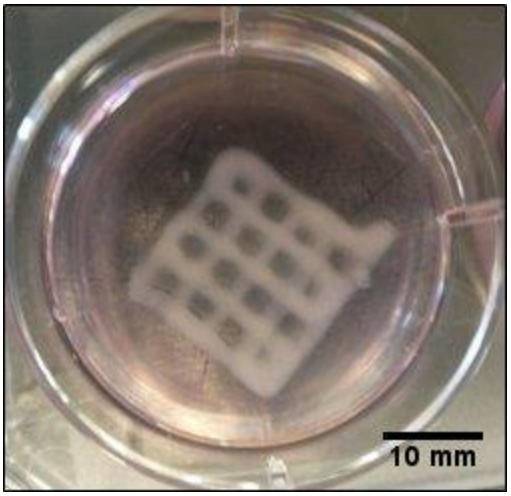

Fig. 13: A printed construct with encapsulated mouse islets and EPCs in core and shell, respectively (representative print quality). Construct has been imaged directly after crosslinking during culture in islet medium. Recorded with conventional camera.

5.5.1 Islet and EPC survival

Primarily, it was investigated whether primary EPCs and islets would survive the printing and crosslinking process. Constructs containing islets, EPCs or both were fabricated and live/dead staining was performed at t = 1 and t = 3 days with FDA/PI. Additionally, free-floating islets in culture medium were included as a positive control. Originally, all images were intended to be recorded through confocal microscopy. However, substantial green background fluorescence was present across all images of printed constructs. This suggests that FDA was retained in the scaffolds in spite of PBS washes post-staining. As a result, the encapsulated islets and EPCs became impossible to image through confocal microscopy with reasonable quality and these were imaged through normal fluorescence microscopy. Signal to noise ratio was still relatively low, but noise has been filtered out as far as possible without affecting representativity. Examples of unfiltered images can still be found in the supplemental figures (**Fig. S3**).

At both t = 1 and t = 3 days, free islets appeared as expected[104] (**Fig. 14D** and **15D**). Diameters of islets were in normal range (50 – 250 µm) and had spherical or slightly elliptical morphologies. Islet cells were predominantly alive, with a few individual dead cells reflected as red spots in the islets. Some smaller fragments (<50 µm, smaller than islet size) were additionally observed alongside islets, which were identified as potentially either residual exocrine pancreatic debris or islet fragments.

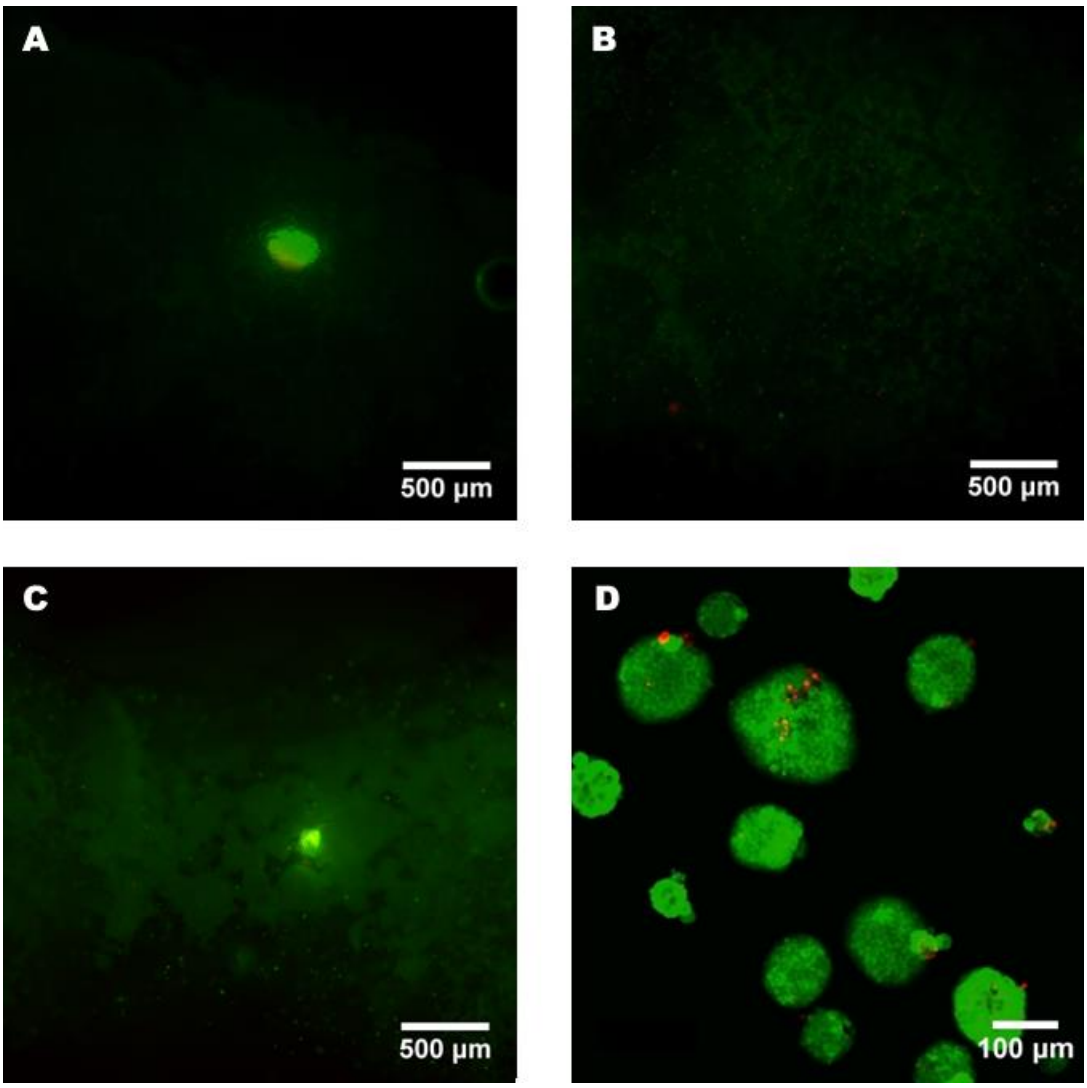

Fig. 14: Live/dead-staining (FDA/PI) of encapsulated and consecutively printed mouse islets (**A**), EPCs (**B**), islets and EPCs (**C**) or free-floating islets in culture medium (**D**) at t = 1 days post-printing. Images recorded through fluorescence microscopy (**A-C**) and confocal microscopy (**D**).

Due to low signal to noise ratio in the scaffolds, individual live or dead cells could not be visualised in printed islets at t = 1 or t = 3 days (**Fig. 14A** and **14C** and **Fig. 15A** and **15C**). However, printed islets still appeared predominantly green. Islets thus appear to survive printing and crosslinking procedures at one day after printing in at least short-term culture post printing.

It proved particularly troubling to visualise EPCs as their fluorescence was only marginally larger than background. Thus, less noise could be filtered from images incorporating EPCs (**Fig. 14B** and **14C** and **15B** and **15C**). However, small specks can still be observed throughout these constructs at both t = 1 and t = 3 days revealing EPCs survived printing and crosslinking. At t = 1 days EPCs were present in single cells and no noticeable changes in morphology could be observed within the short time frame at t = 3 days. It needs to be mentioned, however, that any conclusions are quite limited due to the quality of the images. As no red staining is observed however, the images suggest there are few necrotic EPCs.

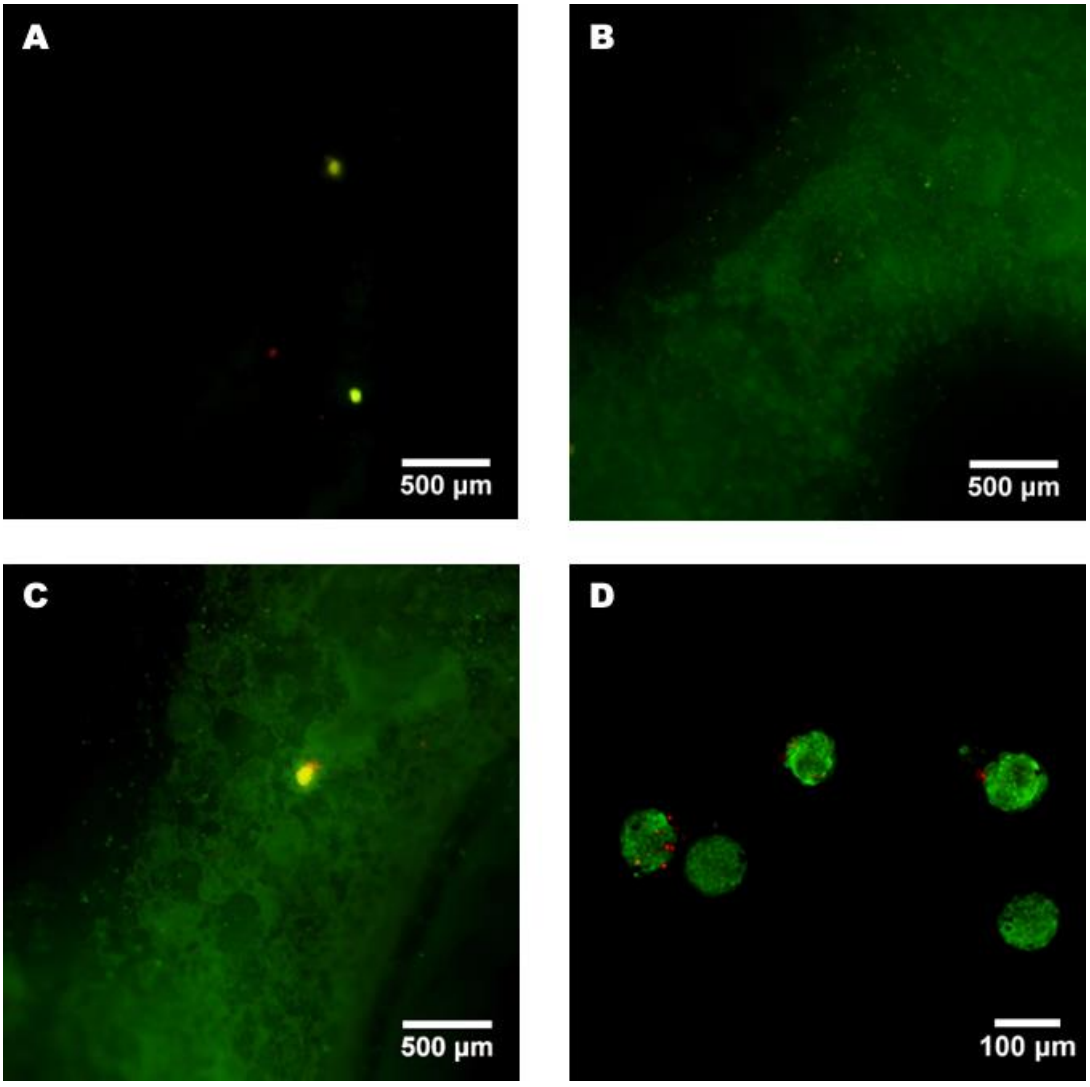

Fig. 15: Live/dead-staining (FDA/PI) of encapsulated and consecutively printed mouse islets (**A**), EPCs (**B**), islets and EPCs (**C**) or free-floating islets in culture medium (**D**) at t = 3 days post-printing. Images recorded through fluorescence microscopy (**A-C**) and confocal microscopy (**D**).

In fibres with encapsulated EPCs and islets, these data suggest that co-printing and short-term co-culture had no detrimental effect on viability for either EPCs or islets at t = 1 and t = 3 days (**Fig. 14C** and **15C**). These recording suggest that islets and EPCs in co-culture appeared similar to those in scaffolds incorporating islets or EPCs alone. Islets were mostly localised at the centre of these fibres,

whereas EPCs were present throughout. Thus, some spatial control in localising islets to centres of fibres was achieved. Whether EPCs were successfully exclusively localised in shell could not be fully concluded due to the nature of fluorescence microscopy and its limited spatial definition along the z-axis. Thus, as the shell envelops the islets in the core entirely, EPCs observed at the centre of the fibres may be above or below the core, but this cannot be fully concluded.

It again needs to be emphasised that the over-all quality of these images is limited, which limits the conclusions that can be reliably drawn from these data alone. Therefore, it is recommended that similar experiments are conducted in the future in order to confirm these preliminary observations. In order to circumvent the present limitations in imaging, the experimental procedures need to be optimised to allow for imaging 3D-printed constructs through confocal microscopy, similar to the depicted free-floating islets depicted in **Fig. 14D** and **Fig. 15D**. The main issue at this stage was background noise, which is hypothesised to be caused by retained FDA in the bioink. To this end, in particular the staining procedures need to be optimised with improved and prolonged washing steps to allow more time for diffusion of FDA out of the printed fibres. If this fails, it may be necessary to resort to a different live cell marker such as calcein AM.

5.5.2 Glucose Stimulated Insulin Secretion

It was next evaluated whether the printed islets also possessed biological functionality. To this end, a series of glucose stimulated insulin secretion (GSIS) experiments was performed at t = 1 and t = 3 days post printing. In two independent experiments consisting of a sample size of three per group, constructs were fabricated as described above with encapsulated islets or islets and EPCs. As a control, free-floating islets were again included in the study. Islets or constructs were first washed in a low glucose buffer and then allowed to recover in low glucose buffer for thirty minutes to allow glucose from culture medium to diffuse out of scaffolds. Next, they were again incubated in a buffer containing low glucose, for sample collection, before being incubated in a buffer with a high concentration of glucose. Insulin secretion in low and high glucose buffers was established with sandwich ELISA.

These results were expressed in terms of a secretion ratio, defined as the concentration of secreted insulin in high glucose divided by the concentration in low glucose. Optimally, in order to compensate for varying amounts of islets in constructs or culture, the secretion would be expressed per DNA or total protein content.[110,113] However, considering the presence of EPCs in one of the groups, this could not be used for these experiments. Nonetheless, the secretion ratio still offers some insight into the glucose response in insulin secretion.

There was a striking degree of variance (within groups) in secretion ratios across all groups (**Fig. 16A**). As such, no significant differences were found between groups or time points, and apparent trends should not be considered conclusive. There are two potential causes for this high variation. First and foremost, it is difficult to control the amounts of islets present in free-floating culture and especially in printed constructs. This can lead to substantial variability in the islet counts.

As the secretion ratio does not reliably compensate for islet number, this is prone to increase variance within groups. Additionally, some debris of sub-islet size (< 50 μm diameter) was observed during islet counts pre-encapsulation, which can also be seen in in the images of free floating islets (**Fig. 14D** and **Fig. 15D**). This debris may consist of islet fragments or exocrine pancreatic cells. One of the functions of exocrine pancreatic cells, is the secretion of digestive enzymes such as proteases. These may cleave insulin, rendering it undetectable by ELISA. The protease-activity and amount of debris is not accounted for in these assays and it is plausible that this varied per sample and experiment. As such, this probably further contributed to the high variance within groups.

Analysis therefore shifted towards the raw data of detected insulin concentrations. As can be expected, similar variance was present within groups in these data (**Fig. 16B** and **16C**). As such, the data are inconclusive for any trends relating to time point or group. It was however observed that all constructs and free-floating islets secrete insulin at levels within the same order of magnitude at both timepoints. Surprisingly, insulin secretion in low glucose conditions was comparable to the secretion in high glucose conditions in the printed islets (with and without co-printed EPCs). This is contrary to the physiological expectations. It is hypothesised that this may be due to the delayed diffusion of glucose from culture medium out of the scaffolds during washing before incubation in low glucose conditions. It is likely that washing time was insufficient for glucose to diffuse out of the scaffolds, resulting in a high-glucose environment from residual glucose despite surrounding buffer with low glucose concentrations. This same effect has been reported elsewhere.[89]

In order to circumvent these limitations, washing steps in the protocol might be lengthened further in order to allow for diffusion as mentioned above. Another alternative would be to digest the scaffolds through the use of enzymes; this has previously been shown to recover glucose response.[89] However, this approach defeats the purpose of the experiment to a major degree, as the main clinical interest is in the glucose response of islets while they are encapsulated. This remains a complex challenge for the construct design. In future construct designs, the best way to improve encapsulated islet GSIS performance, might be to develop functional vasculature. This will be elaborated on in the Future Outlook below.

In conclusion, notwithstanding considerable limitations to the conclusions that can be drawn from the data, it has been shown that printed islets secrete similar (within an order of magnitude) amounts of insulin compared to islets in free-floating culture. Considerable optimisation is still required for better output parameters and additional research is required, but the platform has been shown to allow for islet survival during and shortly after fabrication and it possesses some potential for insulin secretion.

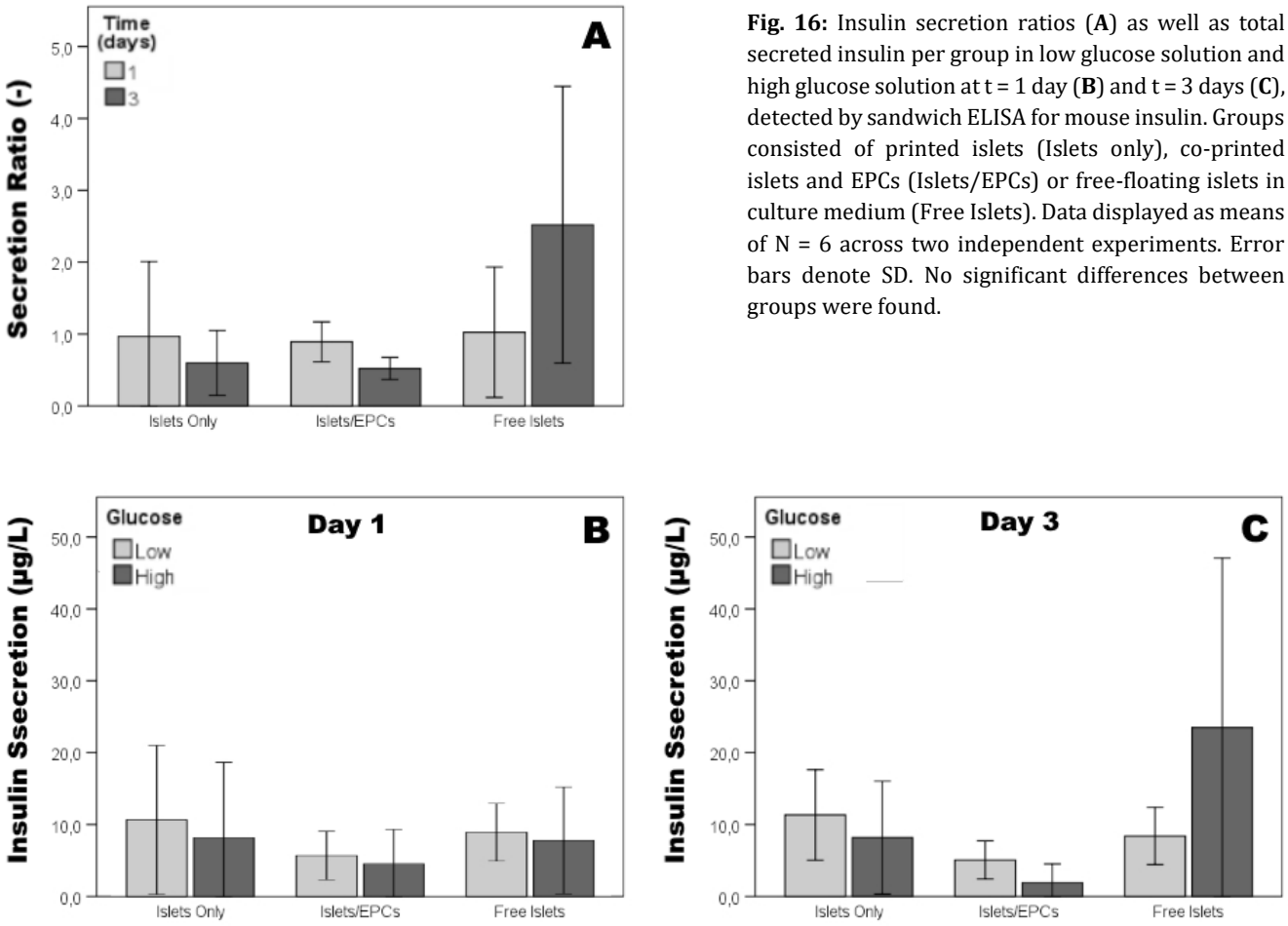

Fig. 16: Insulin secretion ratios (**A**) as well as total secreted insulin per group in low glucose solution and high glucose solution at t = 1 day (**B**) and t = 3 days (**C**), detected by sandwich ELISA for mouse insulin. Groups consisted of printed islets (Islets only), co-printed islets and EPCs (Islets/EPCs) or free-floating islets in culture medium (Free Islets). Data displayed as means of N = 6 across two independent experiments. Error bars denote SD. No significant differences between groups were found.

As mentioned in the platform description in Chapter 3, co-printed EPCs may stimulate islet function. However, this is not apparent in the data here. In the first place, it is expected that this is due to the short culture times. The major advantage of EPCs would be in the development of vascularisation, which expectedly did not occur within three days.

A smaller effect of the presence of endothelial cells is that they affect β-cell behaviour through paracrine signalling[110,111], but these effects have also not been observed. It may be that the three-day time span is similarly insufficient for these effects to take shape, or that the physical separation between EPCs and islets in shell and core fibres with delayed diffusion inhibited paracrine signalling. Most likely, however, the variance within groups was too substantial to detect any (subtle) paracrine signalling effect between islets printed without or with EPCs. It can still be concluded that presence of EPCs did not negatively affect islet viabilities as shown in the previous figures, allowing for these questions to be addressed in follow-up and repeated experiments.

5.5.3 Hypoxia in printed scaffolds

Hypoxic conditions arising due to limited diffusion are one of the central limitations to tissue constructs. For isolated pancreatic islets, oxygen conditions have been shown to be particularly central to islet viability.[114] Therefore, in a final experiment, the degree of hypoxia was investigated in constructs of the same design. However, for easier quantification of data, only EPCs were printed in these constructs. Whereas EPCs were confined to the shell fibres in the previous experiment, EPCs were printed in both core and shell fibres for these experiments in order to obtain a representation of the constructs as a whole.

One day after printing, constructs were cultured in normal conditions in medium supplemented with a marker for cellular hypoxic conditions. A brighter signal corresponds to increased hypoxic conditions. The constructs were imaged with confocal microscopy and compared to hypoxic (1% O_2) and normoxic (unaltered oxygen levels) controls (**Fig. 17**) which consisted of conventional 2D-cell culture.

In the hypoxic control (**Fig. 17A**), cells can be observed clearly with a bright green appearance, as can be expected. Cells appear rounded in single-cell suspension, as cells were trypsinised to allow for imaging. There is a small degree of variability in apparent fluorescence, but this is mainly related to cells situated in a different z-plane resulting in a dimmer appearance. Initially, no signal is apparent in the printed cells (**Fig. 17C**). This would suggest approximately normoxic conditions, considering the similarity with the normoxic control (**Fig. 17B**). However, as fully normoxic conditions throughout the whole construct are unlikely, images were further analysed and signals could be visualised in imaging software with considerably increased contrast (**Fig. S4**). The locations where staining of these cells could be detected with increased contrast have been highlighted with yellow boxes in the unaltered image. Nonetheless, considering the faint signal, these data suggest that conditions are only slightly hypoxic in constructs.

To further elucidate the degree of hypoxia in a more defined manner, quantified data were obtained with flow cytometry (**Fig. 18**). In line with the images displayed in **Fig. 17**, it was established that conditions in constructs were substantially less hypoxic than in hypoxic controls. Interestingly, however, in the quantified data constructs were shown to be significantly different from normoxic control as well, which confirms that conditions are not fully normoxic in constructs as was previously expected. As such, a moderately hypoxic environment is present in the scaffolds. However, based on previous experiments (**Fig. 8, 14** and **15**), it seems that the moderate degree of hypoxia does not affect cell viabilities at least in short-term culture.

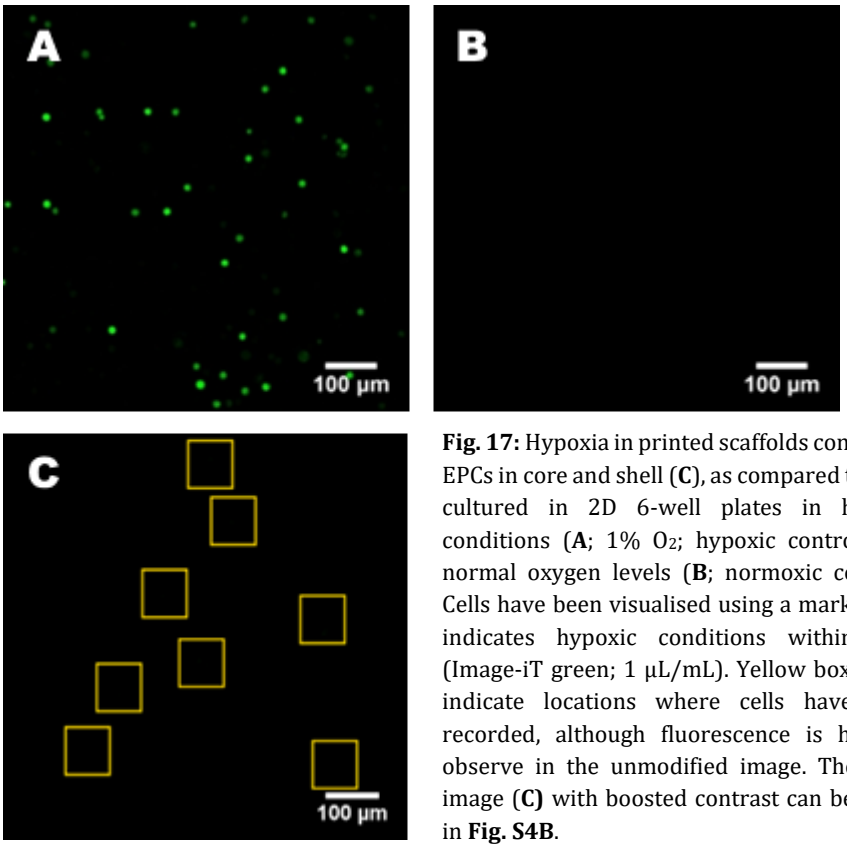

Fig. 17: Hypoxia in printed scaffolds containing EPCs in core and shell (**C**), as compared to EPCs cultured in 2D 6-well plates in hypoxic conditions (**A**; 1% O_2; hypoxic control) and normal oxygen levels (**B**; normoxic control). Cells have been visualised using a marker that indicates hypoxic conditions within cells (Image-iT green; 1 µL/mL). Yellow boxes in **C** indicate locations where cells have been recorded, although fluorescence is hard to observe in the unmodified image. The same image (**C)** with boosted contrast can be found in **Fig. S4B**.

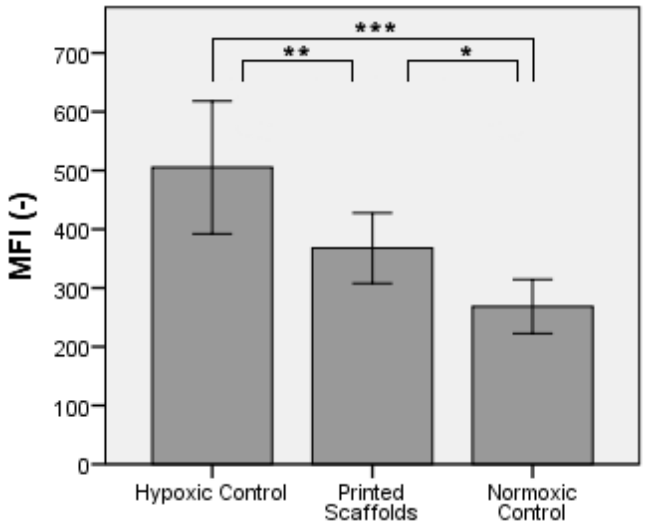

Fig. 18: Hypoxia in printed scaffolds containing EPCs in core and shell, as compared to EPCs cultured in 2D 6-well plates in hypoxic conditions (1% O_2; hypoxic control) and normal oxygen levels (normoxic control). Data have been quantified using flow cytometry, MFI (Mean Fluorescence Intensity) is a measure of hypoxic conditions. Error bars denote the 95% CI. Measurements performed in triplicates. *, ** and *** indicate significant differences at the 0.05, 0.01 and 0.001 levels, respectively.

Chapter 6

6. Discussion

Here, it has been demonstrated that our platform is capable of bioprinting both single cells derived from cell lines and primary islets and EPCs. Although some of the images were of sub-optimal quality, it was seen that printed cells and islets possessed good over-all viability. We have shown that islets secrete insulin, but there was substantial variability in the concentrations of secreted insulin and glucose response was poor. Various limits are present in the current study, which have been summarised below in Table 1.

Various methods have been used in the past to create porous (bio)material scaffolds for 3D-culture of islets, such as lyophilisation[115]. However, in terms of spatial control and definition, these fabrication methods are inferior to Biofabrication as wielded here. The first study applying Biofabrication for endocrine pancreatic tissue engineering is reported in 2011 by Daoud et al.[10] with printed PLGA scaffolds. A drawback of the PLGA material choice is that it is not inherently cell-friendly, which necessitated supplementation of ECM molecules, and its mechanical properties do not match soft tissues. After scaffold fabrication, islets were seeded onto these scaffolds. Seeding of islets after printing may avoid any loss in function or viability of islets induced through shear stress during printing. Due to post-fabrication seeding, however, islets may be localised towards the perimeter of the scaffolds, facilitating immune destruction of islets after transplantation. In another study, direct printing of the β-cells was also avoided by fabricating a potential transplantation device with FDM instead of a tissue construct.[90] However, Marchioli et al. reported the first study where islets and β-cells were directly bioprinted and it was shown that encapsulation and printing of islets was not detrimental to viability.[89] This is in line with what we also show here. To our knowledge, this remains the only study that has investigated the possibility of directly bioprinting β-cells or islets prior to the present thesis.

The study by Marchioli et al. relied on a similar biomaterial choice for the encapsulation and printing of islets as reported here. A hybrid alginate/gelatine bioink was used with slightly different concentrations, but the most considerable distinction in material choice is the methacrylation of gelatine which we have used here. In previous studies[104], it was found that previously used gelatine/alginate blends were dissolved and/or disintegrated *in vivo*. This is likely due to the de-crosslinking and outwash of alginate in the lower concentration calcium environment *in vivo*, paired with the hydrolysis of gelatine. Introducing a double-crosslinked hydrogel network is hypothesised to slow this process down. Although this may require less cell friendly dual crosslinking, we have shown here that this does not noticeably affect viability of β- and endothelial cell lines, primary EPCs or primary islets.

Table 1: Limits to the present study

Description of limitation	Description of proposed solution(s) and / or future outlook
Limited temperature control of bioink, leading to lower viscosity with less spatial control in ink deposition (p. 32)	Temperature control of the bioink was somewhat challenging in this first design iteration of DICAB-1. Printing was feasible with some additional measures (see 5.1.3), but this still resulted in limited control over pore size and constraints on construct size (number of layers). In next iterations of DICAB, improved design of temperature control units will improve control over bioink viscosity, improving over-all print performance.
No formation of MS1 or EPC endothelial cell network (p. 34 and p. 43, respectively)	In encapsulation experiments with MS1 cells, no continuous endothelial cell network formation was observed in spite of high proliferation and good cell viability. In future experiments, VEGF concentrations may be optimised and visualisation needs to be improved with methods such as confocal microscopy to study functional endothelial cell network formation. In printed constructs, EPCs remained in single cell suspension and showed limited bioactivity, with no cell spreading or endothelial network formation. This is due to the limited culture times of only several days. In the future, constructs should be cultured for several weeks to investigate bioactivity of EPCs. These limitations entail that it is currently unproven whether the platform can support the formation of endothelial cell networks and this needs to be further investigated.
CD31 staining was not detected (p. 38)	In the future, a clinically and biologically more relevant cell line with lower passage number may be used, which is less likely to have lost expression of CD31. Using these cells, considerable protocol optimisation should be performed to ensure the staining procedure functions optimally. Finally, the lack of expression could be due to the downregulation of CD31 given the low density of cells within the construct or the absence of junctions, however this seems unlikely as root cause as in 2D-cell culture with high cell density no staining was observed either.
Limited imaging quality of printed constructs containing islets and EPCs (p. 41)	Whether EPCs were successfully, exclusively localised in the shell of printed fibres could not be concluded due to the nature of fluorescence microscopy and its limited spatial definition along the z-axis. Moreover, visualisation of EPCs was of limited quality due to substantial background fluorescence. Therefore, it is recommended experiments are conducted in the future that circumvent the present limitations in imaging. Experimental procedures need to be optimised to allow for imaging 3D-printed constructs through confocal microscopy. In addition, in particular the staining procedures need to be optimised with improved and prolonged washing steps to allow more time for diffusion of FDA out of the printed fibres or alternative staining procedures need to be considered altogether with e.g. calcein AM.
Limited validation of islet/EPC survival (p. 42)	In this manuscript, only qualitative evidence of printed islet and EPC survival is provided. To further substantiate the biocompatibility of the printing process and the bioink with biologically relevant cells, cell viability needs to be quantified for example with Fluorescence-Activated Cell Sorting (FACS). Protocols thereto will require substantial optimisation with respect to scaffold digestion with proteolytic enzymes to break down the GelMA network and ionic de-crosslinking of the alginate network with Ca^{2+}-low media, followed by several washing steps. Optimally, culture times of scaffolds should be extended to several weeks for these experiments.
High variance in glucose secretion in GSIS experiments (p. 46)	Due to excessive within-group variance in GSIS experiments, no significant differences were found between groups or time points, and apparent trends should not be considered conclusive. In order to improve experimental set-up to better assess GSIS, various challenges need to be tackled: a) The amounts of islets present in free-floating culture and especially in printed constructs should be controlled and/or accounted for, in order to express secreted insulin per islet in each construct. b) Filtration steps prior to encapsulation into bioink need to be performed to remove debris of sub-islet size (< 50 µm diameter) which may contain exocrine pancreatic tissue (potentially secreting proteolytic enzymes degrading secreted insulin) c) More extensive washing procedures should be integrated in the experimental protocols to allow for glucose diffusion in and out of scaffolds, such that low- and high-glucose equilibrium is reached in scaffolds prior to assessing insulin secretion.

Encapsulating pancreatic islets for pancreatic tissue engineering remains an active field of study. Nonetheless, a major hurdle that needs to be overcome before Biofabricated scaffolds with encapsulated islets can move to the clinic, is the glucose-responsivity of the insulin secretion. An established minimum for islets to be considered functional is a stimulation index or secretion ratio of 2 or more.[89,116] We report substantial mean concentrations of secreted insulin (albeit with considerable variability) of printed islets; for example three to four fold higher than reported by Marchioli et al. in comparable experiments.[89] Nonetheless, insulin secretion in high glucose was similar to that in low glucose with neither printed islets nor co-printed islets and EPCs reaching mean secretion ratios above 1. This is a persistent issue in 3D-printed islets. None of the studies discussed so far were able to reach the threshold of secretion ratios or stimulation indices above 2 in printed constructs. Although calcium signalling plays a major role in β-cell insulin secretion, it is unlikely to be a dominant cause of lower secretion ratios. Low secretion ratios were similarly observed in constructs crosslinked with other divalent ions[89] and without ionic crosslinking[10,89]. We and other studies therefore hypothesise that lower glucose sensitivity is rather caused by a delayed diffusion of glucose into and out of scaffolds, which is further supported by the observation that islet function is restored upon re-isolation from scaffolds.[89]

Although micro-extrusion of encapsulated islets in itself is not new, it is for the first time reported here that islets can be co-printed with an additional endothelial cell type. Due to the co-axial nozzle set-up, no additional encapsulation steps were required with the same bioink, limiting the handling of islets and exposure to radicals and toxic photo-initiator in hydrogels pre-crosslinking. The data from MS1 cell encapsulation experiments support that the bioink developed here can support the viability and biological activity of endothelial cells during longer culture. It is therefore expected that in this platform vascular structures may be formed with EPCs in longer term culture to supply nutrients and oxygen to the islets. The development of such vasculature may then in turn overcome the limitations to glucose responses associated with delays in diffusion described above.

In a follow-up study by Marchioli et al. in 2016, the glucose diffusion limit leading to decreased islet functionality was also attempted to be overcome through the development of vascularisation.[117] To this end, VEGF was immobilised on heparin-coated PCL discs surrounding islets encapsulated in alginate. Increased development of neovascularisation was observed and islets were substantially more functional with higher stimulation indices. These findings support the notion that improved vascularisation over longer-term culture in the constructs may enhance islet function *in vivo* in the future in this platform as well. Our platform offers an added benefit in that these constructs may be fabricated in a single step through co-axial extrusion, whereas those proposed by Marchioli et al. require several additional steps with increased fabrication times.

Although vascularisation is likely to increase glucose-dependent insulin responses, an additional complication that arises is that it also exposes islets to the host immune system after anastomosis. In light of this, a few macro-encapsulation strategies have attempted to combine development of

vascularisation with immune-shielding by incorporating two membranes[118,119]. The outer membrane would have pores that are large enough to allow for vascularisation, whereas the inner membrane pore size would be small enough to block even humoral immune agents. Nonetheless, this considerably complicates the fabrication process and the second membrane for shielding is still likely to slow down diffusion. For our platform, we therefore envision an alternative strategy in the future that may resolve the threat of immune-destruction enabled by vascularisation, which will be elaborated on in the future outlook below.

It becomes apparent that the central benefit of the proposed platform here is the relatively simple fabrication, while still allowing for the co-delivery of islets and endothelial cells through co-axial extrusion. Co-axial micro-extrusion has been used previously for various applications, including for endocrine pancreatic engineering in 2015, where hollow alginate tubes were fabricated by extruding sodium alginate through a shell nozzle with crosslinking solution in the core.[88] The tubes were consecutively used for the culturing of tissue strands incorporating β-TC3 cells or fibroblasts. Here, it has been demonstrated that co-axial extrusion cannot be used only for the fabrication of a culture mould, but even for direct co-printing of β-cells or islets with endothelial cells, in a single-step fabrication.

In one of the additional experiments performed here, the degree of hypoxia throughout the constructs was evaluated. It is well established that hypoxia has a major detrimental effect on islet viability and function. Based on viabilities post printing and during culture, it was already expected that hypoxia would be minor. This was confirmed qualitatively and quantitatively. Nonetheless, it needs to be mentioned that these constructs only consisted of a single layer, and it can be expected that hypoxia may increase moderately as construct sizes increase with additional layers. Conversely, the development of vascularisation, which the proposed bioink supports as the data suggest here, can be expected to counter-act this in the longer term in culture.

Chapter 7

7. Future Outlook

Several central hurdles still exist for the field of Biofabrication at large, such as the reliable development of vascular trees and innervation as well as standardisation of procedures and scalability. These future directions have been elaborately described elsewhere and will not be repeated further here.[31,82] However, based on the data presented here, various recommendations can be made towards the future progress of this project in particular. Here, some short recommendations for follow-up experiments will be touched upon as well as some recommendations towards future standardisation and optimisation of several parameters in the platform. Finally, it will be envisioned how an ultimate construct design from this platform could take shape that meets all requirements identified at the start of this thesis (**Fig. 1**).

7.1 Follow-up experiments

In this thesis, it has been described that endothelial cells show substantial cell spreading and alignment after three weeks of culture. This demonstrates that cells survive in the material for longer culture durations and suggests that the hydrogel may support the development of functional vascularisation in the future. However, to conclusively demonstrate the latter, additional experiments are required with also clinically more relevant cell types. It is recommended that commercially available angiogenesis assays are performed with for example HUVECs (human umbilical cord endothelial cells) or EPCs. It should then also be confirmed that the printing process does not affect angiogenesis and it may be interesting to compare printed and mould-casted constructs in light of this. In order to fully confirm functionality of observed structures, it is additionally recommended that lumen formation is visualised with confocal microscopy.

Some initial insight has been offered here into the establishment of an MS1/β-TC-6 co-culture as a model system. Although a quantifiable indication has been established of the relative metabolism and proliferation of these cell types and a suitable co-culture medium has been found, this co-culture system could be further optimised by attempting various cell encapsulation/printing ratios and tracking cell survival of both cell types over time. It may be argued that a cell line based co-culture platform has become obsolete since compatibility of the platform with more relevant cells including primary islets and EPCs has been confirmed. Taking some ethical considerations in mind, however, further development of the co-culture platform with cell lines may be useful for future, more preliminary, optimisation and platform developing experiments to limit animal use and it will be considerably more cost-effective for these experiments. It needs to be pointed out that for further optimisation of the co-culture platform, a more sophisticated experimental set-up may be necessary than used here. The experiment here was only designed to offer an indication, whereas more accurate cell counts and viability counts may be obtained for example with flow cytometry in the future.

Tying in with these co-culture considerations, it was attempted here to track MS1 and β-TC-

6 cell fate to some degree through fluorescent labelling of CD31 on MS1 cells. This was ultimately unsuccessful. Establishing a functional protocol for distinguishing these cells will be required for tracking their fates independently. Additionally, this could confirm the successful localisation of the different cell types to core and shell fibres, which to date has only been confirmed reliably for labelled bioink without encapsulated cells.

One of the key findings here is that primary islets survive encapsulation, printing and crosslinking, which is the first and essential step in the development of this platform for endocrine pancreatic tissue engineering. Nonetheless, it generates more questions than it answers. Essential follow-up questions will be whether islets survive longer term culture in the constructs of several weeks or whether the moderate hypoxia and hypothesised delayed nutrient diffusion will lead to necrotic core formation at the construct or islet level after such time.

Additionally, major variance in insulin secretion and glucose response are reported here. It needs to be established whether these can be diminished. One suggestion to this end is to filter isolated islets with a 40-μm filter and discard the filtrate, which will contain apoptotic islet fragments and protease-secreting remnants of the exocrine pancreata. As previously mentioned, the inconsistent presence of especially exocrine cells between samples is hypothesised to have made a major contribution to the observed variance. Additionally, methods can be devised to express secretion in stimulation indices by compensating for islet count. This may be a complicated endeavour nonetheless, considering the presence of additional cell types in some groups. This renders a total protein or DNA count an inadequate measure for islet count. At the present time, no method was yet available for such compensation. A manual count of islets per construct may be an option with light or confocal microscopy, but this may be time-consuming, labour-intensive, subjective and moderately unreliable.

As a final recommendation for a follow-up experiment, some more investigation into the hypoxia in scaffolds may be interesting. Here, EPCs were printed in both core and shell fibres and then collectively assessed for hypoxic conditions, offering a picture of hypoxia in the scaffold as a whole. The same experiments can be conducted with EPCs printed exclusively in core or shell, which will demonstrate if there is a significant difference in hypoxia between the core and shell fibres, which will offer some additional insight into the efficiency of oxygen diffusion into the constructs. Furthermore, as different cell types are differently affected by hypoxic conditions, it may be interesting to repeat these experiments with β-cells or islets.

7.2 Standardisation and optimisation

For this thesis, a broad range of different experiments has been performed in a moderately limited amount of time. Although this resulted in several useful proof-of-concepts, the time restriction led to some experiments being performed with parameters established through trial and error, rather than systematic optimisation. Considering the collaboration between the different institutions,

standardisation and optimisation is required for the progress of the project.

Primarily, the preparation and handling of the bioink needs to be optimised and standardised. It was observed that there was substantial variability in preparation methods between researchers from the different institutes, in addition to the use of different suppliers for some of the reagents. Although some batch to batch variability is unavoidable, in part due to variability in different batches of prepared GelMA for example, bioink behaviour was observed to vary substantially between batches. For example, it was reported here that substantial a-specific staining of bioink was consistently observed with FDA, whereas previous studies reported no such observations in spite of similar staining procedures.[104] Additional parameters for bioink handling that need to be optimised and standardised are crosslinking time (ionic and photo-crosslinking), light intensity and distance (photo-crosslinking) and photo-initiator concentrations. These parameters need to be optimised for cellular response and mechanical properties. Additionally, it can be optimised for scaffold porosity and interconnectivity after crosslinking. Although some insight has been offered previously through SEM[104], SEM has a major impact on the microstructure of hydrated samples and does not accurately represent porosity in hydrated conditions. A useful alternative may be to investigate the hydrogel microstructure through scanning electron cryomicroscopy (SECM), which avoids distortion from dehydration. SECM would be a suitable method to investigate pore sizes across different crosslinking parameters, which can then be optimised.

Finally, additional standardisation can be performed for printing procedures. Particularly, bioink temperatures during printing were only defined by system settings, which were expected to vary substantially from actual cartridge temperatures. This was further exacerbated by intermittent placing on ice during the islet printing experiments for additional cooling. Although DICAB-1 at the time of writing of this thesis has become obsolete with the arrival of the next generation (DICAB-2) with improved temperature regulation, it is necessary that the cartridge temperatures for this new system are accurately identified as related to the system temperature settings for reproducibility. Additionally, some of the standardisations and characterisations performed here for DICAB-1 will need to be repeated for DICAB-2.

7.3 Future construct design

At the start of this thesis, the requirements for a successful tissue engineered and/or Biofabricated construct of the endocrine pancreas were identified (**Fig. 1**). The construct design as presented in the final experiments described here, can be seen to only partially fulfil these requirements. First, it meets a requirement in that it allows for sufficient diffusion of oxygen and nutrients for cell and islet survival based on the hypoxia experiments and viabilities in fibres and constructs. Second, it has been shown that endothelial cells survive sufficiently long and in future experiments more steps can be made towards development of vascularisation (the second identified requirement). The two requirements for a successful endocrine pancreatic tissue construct that are wholly lacking in the present construct design are glucose sensitivity and immune-protection.

A future construct design has been envisioned which may live up to all the requirements (**Fig. 19**). This design will be the convergence of this project in the present thesis and several projects running in parallel at the University of Adelaide. To provide immune-protection, T-regs may be incorporated into the tissue construct to stimulate tolerogenesis. T-reg behaviour in the GelMA/alginate bioink is currently being investigated at the University of Adelaide. Further, it will be beneficial to incorporate EPCs in both core and shell fibres to allow for development of vascularisation throughout the construct. Although EPCs were contained in the shell here as a proof of concept, fully-developed vascularisation through core and shell could enable increased diffusion rates, which in turn may increase GSIS and will positively affect islet survival. Islets would still be incorporated in the core, whereas T-regs may be localised in the shell of the fibres. The constructs could then still be fabricated in a single printing step by depositing the fibres in x/y-grids and stacking into several layers. If T-reg tolerogenesis and formation of vascularisation can then be optimised, a construct design may be feasible which meets all requirements.

As a final remark, it needs to be noted that the application of this design would still be limited as the general shortage in allogeneic islets would still prevent wide-scale application. This may be circumvented by using pseudo-islets or islet-like organoids derived from ESCs or iPSCs in an ultimate construct design. Major steps have been made in developing these tissues and optimising their GSIS.[42–45,120] As an additional advantage of this construct design, the risks associated with their use (for example teratoma formation) may be more limited due to the encapsulation and thereby retrievability of the pseudo-islets in the constructs.

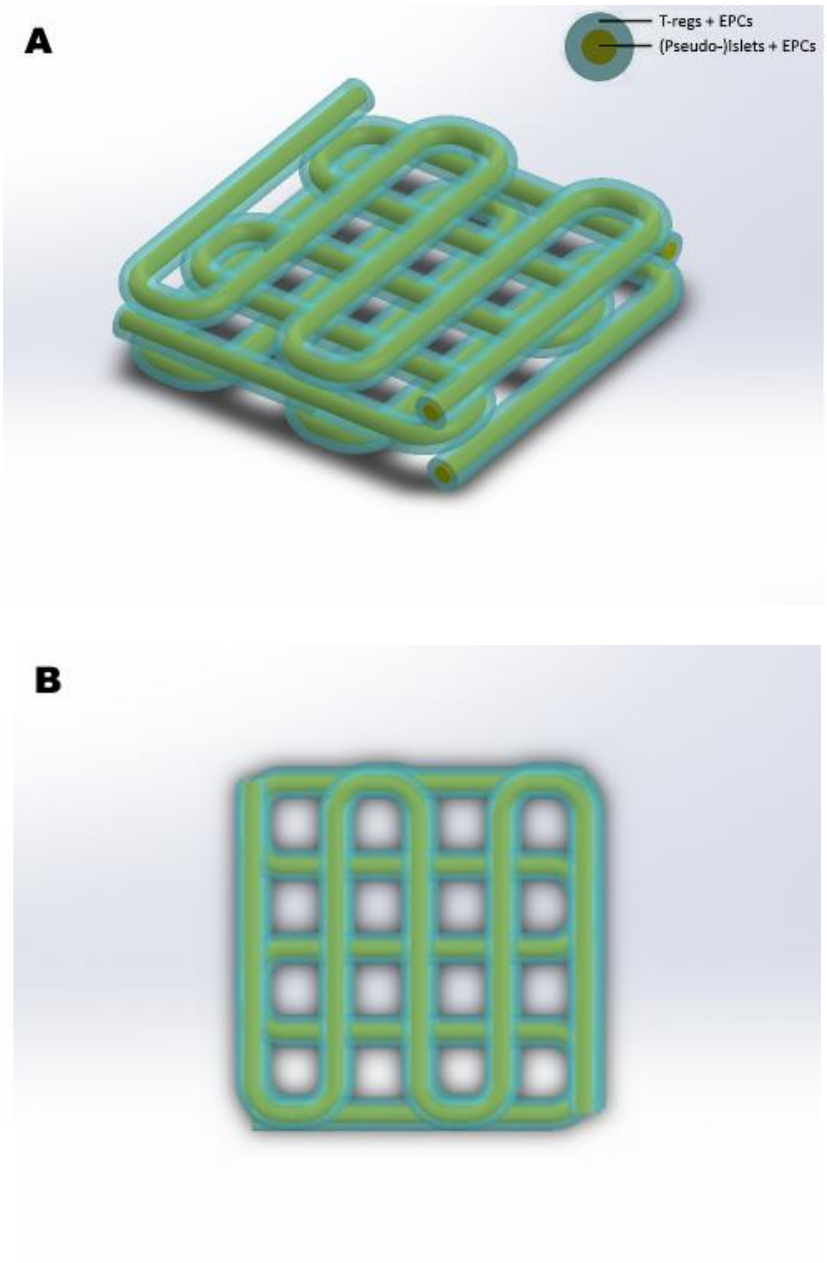

Fig. 19: A schematic representation of a potential future construct design, which may meet all requirements for a successful Biofabricated endocrine pancreatic tissue construct. A top-view is provided in **B**. Tregs and EPCs would be located in the shell of the fibres (blue), (pseudo-)islets and EPCs would be located in the core of the fibres (green). Shells would be stacked into a multi-layered construct.

Chapter 8

8. Conclusion

A platform for the fabrication of endocrine pancreatic tissue constructs through co-axial micro-extrusion was developed. It was shown that the custom printing set-up, DICAB-1, can print co-axial fibres with Pluronic as well as GelMA/alginate bioink, and is capable of printing both β-cell lines and endothelial cell lines with good viability. It was further demonstrated in encapsulation experiments that the GelMA/alginate bioink can sustain long-term culture and steps have been made towards developing a co-culture platform of MS1 endothelial and β-TC-6 cells.

In addition, primary murine islets and isolated endothelial progenitor cells have been printed into core/shell-constructs with good viability. Islets were shown to secrete substantial amounts of insulin. The degree of hypoxia in printed scaffolds has been evaluated qualitatively and quantitatively; it was found that conditions were mildly hypoxic but this did not appear to have affected short-term islet viability in earlier experiments. However, glucose response of printed islets was poor. A potential construct design in the future is however envisioned which may improve insulin secretion dynamics and provide immune-protection through tolerogenesis, thus meeting all requirements for an optimal, tissue engineered endocrine pancreatic tissue construct fabricated in a single step.

References

1. Centre for Disease Control and Prevention. *Diabetes report card*. (2014).
2. Cade, W. T. Diabetes-Related Microvascular and Macrovascular Diseases in the Physical Therapy Setting. *Phys. Ther.* **88,** 1322–1335 (2008).
3. Laing, S. P. *et al.* Mortality from heart disease in a cohort of 23,000 patients with insulin-treated diabetes. *Diabetologia* **46,** 760–765 (2003).
4. Umpierrez, G. E., Murphy, M. B. & Kitabchi, A. E. Diabetic Ketoacidosis and Hyperglycemic Hyperosmolar Syndrome. *Diabetes Spectr.* **15,** 28–36 (2002).
5. Atkinson, M. A., Eisenbarth, G. S. & Michels, A. W. Type 1 diabetes. *Lancet* **383,** 69–82 (2014).
6. MacNeil, S. Progress and opportunities for tissue-engineered skin. *Nature* **445,** 874–880 (2007).
7. Raya-Rivera, A. *et al.* Tissue-engineered autologous urethras for patients who need reconstruction: an observational study. *Lancet* **377,** 1175–1182 (2011).
8. Mumme, M. *et al.* Nasal chondrocyte-based engineered autologous cartilage tissue for repair of articular cartilage defects: an observational first-in-human trial. *Lancet* **388,** 1985–1994 (2016).
9. Tziampazis, E. & Sambanis, A. Tissue Engineering of a Bioartificial Pancreas: Modeling the Cell Environment and Device Function. *Biotechnol. Prog.* **11,** 115–126 (1995).
10. Daoud, J. T. *et al.* Long-term in vitro human pancreatic islet culture using three-dimensional microfabricated scaffolds. *Biomaterials* **32,** 1536–1542 (2011).
11. Novosel, E. C., Kleinhans, C. & Kluger, P. J. Vascularization is the key challenge in tissue engineering. *Adv. Drug Deliv. Rev.* **63,** 300–311 (2011).
12. Auger, F. A., Gibot, L. & Lacroix, D. The Pivotal Role of Vascularization in Tissue Engineering. *Annu. Rev. Biomed. Eng.* **15,** 177–200 (2013).
13. Groll, J. *et al.* Biofabrication: reappraising the definition of an evolving field. *Biofabrication* **8,** 013001 (2016).
14. Leung, P. S. Physiology of the Pancreas. in 13–27 (Springer, Dordrecht, 2010). doi:10.1007/978-90-481-9060-7_2
15. Bluestone, J. A., Herold, K. & Eisenbarth, G. Genetics, pathogenesis and clinical interventions in type 1 diabetes. *Nature* **464,** 1293–1300 (2010).
16. Menge, B. A. *et al.* Partial pancreatectomy in adult humans does not provoke beta-cell regeneration. *Diabetes* **57,** 142–9 (2008).
17. Rankin, M. M. & Kushner, J. A. Adaptive beta-cell proliferation is severely restricted with advanced age. *Diabetes* **58,** 1365–72 (2009).
18. Shah, R. B., Patel, M., Maahs, D. M. & Shah, V. N. Insulin delivery methods: Past, present and future. *Int. J. Pharm. Investig.* **6,** 1–9 (2016).
19. Steffes, M. W. *et al.* Sustained effect of intensive treatment of type 1 diabetes mellitus on development and progression of diabetic nephropathy: the Epidemiology of Diabetes

Interventions and Complications (EDIC) study. *JAMA* **290,** 2159–67 (2003).

20. Stadler, M. *et al.* Long-Term Mortality and Incidence of Renal Dialysis and Transplantation in Type 1 Diabetes Mellitus. *J. Clin. Endocrinol. Metab.* **91,** 3814–3820 (2006).
21. Maahs, D. M. & Rewers, M. Mortality and Renal Disease in Type 1 Diabetes Mellitus - Progress Made, More to Be Done. *J. Clin. Endocrinol. Metab.* **91,** 3757–3759 (2006).
22. Mannucci, E., Monami, M., Dicembrini, I., Piselli, A. & Porta, M. Achieving HbA1c targets in clinical trials and in the real world: a systematic review and meta-analysis. *J. Endocrinol. Invest.* **37,** 477–495 (2014).
23. Kelly, W. D., Lillehei, R. C., Merkel, F. K., Idezuki, Y. & Goetz, F. C. Allotransplantation of the pancreas and duodenum along with the kidney in diabetic nephropathy. *Surgery* **61,** 827–37 (1967).
24. Frank, A. *et al.* Transplantation for type I diabetes: comparison of vascularized whole-organ pancreas with isolated pancreatic islets. *Ann. Surg.* **240,** 631-40; discussion 640–3 (2004).
25. Venstrom, J. M. *et al.* Survival After Pancreas Transplantation in Patients With Diabetes and Preserved Kidney Function. *JAMA* **290,** 2817 (2003).
26. Barton, F. B. *et al.* Improvement in outcomes of clinical islet transplantation: 1999-2010. *Diabetes Care* **35,** 1436–45 (2012).
27. Shapiro, A. M. J. *et al.* Islet Transplantation in Seven Patients with Type 1 Diabetes Mellitus Using a Glucocorticoid-Free Immunosuppressive Regimen. *N. Engl. J. Med.* **343,** 230–238 (2000).
28. Gala-Lopez, B. *et al.* Microbial Contamination of Clinical Islet Transplant Preparations Is Associated with Very Low Risk of Infection. *Diabetes Technol. Ther.* **15,** 323–327 (2013).
29. Lim, F. & Sun, A. M. Microencapsulated islets as bioartificial endocrine pancreas. *Science* **210,** 908–10 (1980).
30. Desai, T. & Shea, L. D. Advances in islet encapsulation technologies. *Nat. Rev. Drug Discov.* **16,** 338–350 (2017).
31. Murphy, S. V & Atala, A. 3D bioprinting of tissues and organs. *Nat. Biotechnol.* **32,** 773–785 (2014).
32. Parnaud, G. *et al.* Proliferation of sorted human and rat beta cells. *Diabetologia* **51,** 91–100 (2007).
33. Talchai, C., Xuan, S., Lin, H. V., Sussel, L. & Accili, D. Pancreatic β Cell Dedifferentiation as a Mechanism of Diabetic β Cell Failure. *Cell* **150,** 1223–1234 (2012).
34. Merglen, A. *et al.* Glucose Sensitivity and Metabolism-Secretion Coupling Studied during Two-Year Continuous Culture in INS-1E Insulinoma Cells. *Endocrinology* **145,** 667–678 (2004).
35. Ravassard, P. *et al.* A genetically engineered human pancreatic β cell line exhibiting glucose-inducible insulin secretion. *J. Clin. Invest.* **121,** 3589–97 (2011).
36. Groth, C. . *et al.* Transplantation of porcine fetal pancreas to diabetic patients. *Lancet* **344,** 1402–1404 (1994).
37. Pellegrini, S., Cantarelli, E., Sordi, V., Nano, R. & Piemonti, L. The state of the art of islet

transplantation and cell therapy in type 1 diabetes. *Acta Diabetol.* **53,** 683–691 (2016).

38. Dufrane, D. & Gianello, P. Pig islet for xenotransplantation in human: structural and physiological compatibility for human clinical application. *Transplant. Rev.* **26,** 183–188 (2012).
39. Elliott, R. B. *et al.* Live encapsulated porcine islets from a type 1 diabetic patient 9.5 yr after xenotransplantation. *Xenotransplantation* **14,** 157–161 (2007).
40. Thompson, P. *et al.* Islet Xenotransplantation Using Gal-Deficient Neonatal Donors Improves Engraftment and Function. *Am. J. Transplant.* **11,** 2593–2602 (2011).
41. Patience, C., Takeuchi, Y. & Weiss, R. A. Infection of human cells by an endogenous retrovirus of pigs. *Nat. Med.* **3,** 282–286 (1997).
42. Lumelsky, N. *et al.* Differentiation of Embryonic Stem Cells to Insulin-Secreting Structures Similar to Pancreatic Islets. *Science (80-.).* **292,** 1389–1394 (2001).
43. Pagliuca, F. W. *et al.* Generation of Functional Human Pancreatic β Cells In Vitro. *Cell* **159,** 428–439 (2014).
44. Rezania, A. *et al.* Reversal of diabetes with insulin-producing cells derived in vitro from human pluripotent stem cells. *Nat. Biotechnol.* **32,** 1121–1133 (2014).
45. Millman, J. R. & Pagliuca, F. W. Autologous Pluripotent Stem Cell–Derived β-Like Cells for Diabetes Cellular Therapy. *Diabetes* **66,** 1111–1120 (2017).
46. Jacobson, E. F. & Tzanakakis, E. S. Human pluripotent stem cell differentiation to functional pancreatic cells for diabetes therapies: Innovations, challenges and future directions. *J. Biol. Eng.* **11,** 21 (2017).
47. Espes, D., Lau, J. & Carlsson, P.-O. Towards the clinical translation of stem cell therapy for type 1 diabetes. *Eur. J. Endocrinol.* **177,** R159–R168 (2017).
48. Hematti, P., Kim, J., Stein, A. P. & Kaufman, D. Potential role of mesenchymal stromal cells in pancreatic islet transplantation. *Transplant. Rev.* **27,** 21–29 (2013).
49. Montanari, E. *et al.* Multipotent mesenchymal stromal cells enhance insulin secretion from human islets via N-cadherin interaction and prolong function of transplanted encapsulated islets in mice. *Stem Cell Res. Ther.* **8,** 199 (2017).
50. Zhou, Q. & Melton, D. A. Pancreas regeneration. *Nature* (2018). doi:10.1038/s41586-018-0088-0
51. Halban, P. a *et al.* The possible importance of contact between pancreatic islet cells for the control of insulin release. *Endocrinology* (1982). doi:10.1210/endo-111-1-86
52. Cabrera, O. *et al.* The unique cytoarchitecture of human pancreatic islets has implications for islet cell function. *Proc. Natl. Acad. Sci.* (2006). doi:10.1073/pnas.0510790103
53. Benninger, R. K. P., Head, W. S., Zhang, M., Satin, L. S. & Piston, D. W. Gap junctions and other mechanisms of cell-cell communication regulate basal insulin secretion in the pancreatic islet. *J. Physiol.* (2011). doi:10.1113/jphysiol.2011.218909
54. Cantarelli, E., Citro, A. & Piemonti, L. Pancreatic Islet Transplantation Technologies: State of the Art of Micro- and Macro-Encapsulation. *Curr. Transplant. Reports* **4,** 169–183 (2017).

55. Omami, M. *et al.* Islet Microencapsulation: Strategies and Clinical Status in Diabetes. *Current Diabetes Reports* (2017). doi:10.1007/s11892-017-0877-0
56. Soon-Shiong, P. *et al.* Insulin independence in a type 1 diabetic patient after encapsulated islet transplantation. *Lancet* **343,** 950–951 (1994).
57. Calafiore, R. *et al.* Microencapsulated pancreatic islet allografts into nonimmunosuppressed patients with type 1 diabetes: first two cases. *Diabetes Care* **29,** 137–8 (2006).
58. Tuch, B. E. *et al.* Safety and Viability of Microencapsulated Human Islets Transplanted Into Diabetic Humans. *Diabetes Care* **32,** 1887–1889 (2009).
59. Basta, G. *et al.* Long-term metabolic and immunological follow-up of nonimmunosuppressed patients with type 1 diabetes treated with microencapsulated islet allografts: four cases. *Diabetes Care* **34,** 2406–9 (2011).
60. Desai, T. A., West, T., Cohen, M., Boiarski, T. & Rampersaud, A. Nanoporous microsystems for islet cell replacement. *Adv. Drug Deliv. Rev.* **56,** 1661–1673 (2004).
61. Sneddon, J. B. *et al.* Stem Cell Therapies for Treating Diabetes: Progress and Remaining Challenges. *Cell Stem Cell* **22,** 810–823 (2018).
62. Desai, T. A. *et al.* Microfabricated Biocapsules Provide Short-Term Immunoisolation of Insulinoma Xenografts. *Biomed. Microdevices* **1,** 131–138 (1999).
63. Chang, R. *et al.* Nanoporous Immunoprotective Device for Stem-Cell-Derived β-Cell Replacement Therapy. *ACS Nano* **11,** 7747–7757 (2017).
64. Shapiro, A. M. J., Pokrywczynska, M. & Ricordi, C. Clinical pancreatic islet transplantation. *Nat. Rev. Endocrinol.* **13,** 268–277 (2017).
65. Posselt, A. M. *et al.* Islet transplantation in type 1 diabetic patients using calcineurin inhibitor-free immunosuppressive protocols based on T-cell adhesion or costimulation blockade. *Transplantation* **90,** 1595–601 (2010).
66. Bombardier, C. *et al.* Comparison of Upper Gastrointestinal Toxicity of Rofecoxib and Naproxen in Patients with Rheumatoid Arthritis. *N. Engl. J. Med.* **343,** 1520–1528 (2000).
67. Rezzani, R. Cyclosporine A and adverse effects on organs: histochemical studies. *Prog. Histochem. Cytochem.* **39,** 85–128 (2004).
68. Marek-Trzonkowska, N. *et al.* Administration of CD4+CD25highCD127- regulatory T cells preserves β-cell function in type 1 diabetes in children. *Diabetes Care* (2012). doi:10.2337/dc12-0038
69. Bluestone, J. A. *et al.* Type 1 diabetes immunotherapy using polyclonal regulatory T cells. *Sci. Transl. Med.* (2015). doi:10.1126/scitranslmed.aad4134
70. Asakawa, N. *et al.* Pre-vascularization of in vitro three-dimensional tissues created by cell sheet engineering. *Biomaterials* **31,** 3903–3909 (2010).
71. Jain, R. K., Au, P., Tam, J., Duda, D. G. & Fukumura, D. Engineering vascularized tissue. *Nat. Biotechnol.* **23,** 821–823 (2005).
72. Jansson, L. *et al.* Pancreatic islet blood flow and its measurement. *Ups. J. Med. Sci.* **121,** 81–95 (2016).

73. Henderson, J. R. & Moss, M. C. A morphometric study of the endocrine and exocrine capillaries of the pancreas. *Q. J. Exp. Physiol.* **70,** 347–56 (1985).
74. Renes, M. J. Biofabrication for Vascularization: A review of current strategies and techniques. (2017).
75. Miller, J. S. *et al.* Rapid casting of patterned vascular networks for perfusable engineered three-dimensional tissues. *Nat. Mater.* **11,** 768–774 (2012).
76. Kolesky, D. B., Homan, K. A., Skylar-Scott, M. A. & Lewis, J. A. Three-dimensional bioprinting of thick vascularized tissues. *Proc. Natl. Acad. Sci. U. S. A.* **113,** 3179–84 (2016).
77. Baldwin, J. *et al.* In vitro pre-vascularisation of tissue-engineered constructs A co-culture perspective. *Vasc. Cell* **6,** 1–16 (2014).
78. Lammert, E. *et al.* Role of VEGF-A in Vascularization of Pancreatic Islets. *Curr. Biol.* **13,** 1070–1074 (2003).
79. Malda, J. *et al.* 25th Anniversary Article: Engineering Hydrogels for Biofabrication. *Adv. Mater.* **25,** 5011–5028 (2013).
80. Bajaj, P., Schweller, R. M., Khademhosseini, A., West, J. L. & Bashir, R. 3D Biofabrication Strategies for Tissue Engineering and Regenerative Medicine. *Annu. Rev. Biomed. Eng.* **16,** 247–276 (2014).
81. Pati, F., Jang, J., Lee, J. W. & Cho, D. W. *Extrusion bioprinting*. *Essentials of 3D Biofabrication and Translation* (Elsevier Inc., 2015). doi:10.1016/B978-0-12-800972-7.00007-4
82. Ozbolat, I. T. & Hospodiuk, M. Current advances and future perspectives in extrusion-based bioprinting. *Biomaterials* **76,** 321–343 (2016).
83. Onoe, H. *et al.* Metre-long cell-laden microfibres exhibit tissue morphologies and functions. *Nat. Mater.* **12,** 584–590 (2013).
84. Attalla, R., Ling, C. & Selvaganapathy, P. Fabrication and characterization of gels with integrated channels using 3D printing with microfluidic nozzle for tissue engineering applications. *Biomed. Microdevices* **18,** 17 (2016).
85. Jia, W. *et al.* Direct 3D bioprinting of perfusable vascular constructs using a blend bioink. *Biomaterials* **106,** 58–68 (2016).
86. Yue, Z., Liu, X., Coates, P. T. & Wallace, G. G. Advances in printing biomaterials and living cells: Implications for islet cell transplantation. *Current Opinion in Organ Transplantation* **21,** 467–475 (2016).
87. Ravnic, D. J., Leberfinger, A. N. & Ozbolat, I. T. Bioprinting and Cellular Therapies for Type 1 Diabetes. *Trends in Biotechnology* **35,** 1025–1034 (2017).
88. Akkouch, A., Yu, Y. & Ozbolat, I. T. Microfabrication of scaffold-free tissue strands for three-dimensional tissue engineering. *Biofabrication* **7,** (2015).
89. Marchioli, G. *et al.* Fabrication of three-dimensional bioplotted hydrogel scaffolds for islets of Langerhans transplantation. *Biofabrication* **7,** (2015).
90. Song, J. & Millman, J. R. Economic 3D-printing approach for transplantation of human stem cell-derived *β* -like cells. *Biofabrication* **9,** 015002 (2016).

91. O'Connell, C. D. *et al.* Development of the Biopen: A handheld device for surgical printing of adipose stem cells at a chondral wound site. *Biofabrication* **8,** (2016).
92. Duchi, S. *et al.* Handheld Co-Axial Bioprinting: Application to in situ surgical cartilage repair. *Sci. Rep.* **7,** (2017).
93. Di Bella, C. *et al.* In situ handheld three-dimensional bioprinting for cartilage regeneration. *J. Tissue Eng. Regen. Med.* **12,** 611–621 (2018).
94. Cornock, R., Beirne, S., Thompson, B. & Wallace, G. G. Coaxial additive manufacture of biomaterial composite scaffolds for tissue engineering. *Biofabrication* **6,** (2014).
95. Taylor, A. C., Beirne, S., Alici, G. & Wallace, G. G. System and process development for coaxial extrusion in fused deposition modelling. *Rapid Prototyp. J.* **23,** 543–550 (2017).
96. Dumortier, G., Grossiord, J. L., Agnely, F. & Chaumeil, J. C. A review of poloxamer 407 pharmaceutical and pharmacological characteristics. *Pharmaceutical Research* (2006). doi:10.1007/s11095-006-9104-4
97. Wu, W., DeConinck, A. & Lewis, J. A. Omnidirectional Printing of 3D Microvascular Networks. *Adv. Mater.* **23,** H178–H183 (2011).
98. Kang, H.-W. *et al.* A 3D bioprinting system to produce human-scale tissue constructs with structural integrity. *Nat. Biotechnol.* **34,** 312–319 (2016).
99. Nichol, J. W. *et al.* Cell-laden microengineered gelatin methacrylate hydrogels. *Biomaterials* **31,** 5536–5544 (2010).
100. Guan, X. *et al.* Development of hydrogels for regenerative engineering. *Biotechnol. J.* 1600394 (2017). doi:10.1002/biot.201600394
101. Rowley, J. A., Madlambayan, G. & Mooney, D. J. Alginate hydrogels as synthetic extracellular matrix materials. *Biomaterials* **20,** 45–53 (1999).
102. Pierschbacher, M. D. & Ruoslahti, E. Cell attachment activity of fibronectin can be duplicated by small synthetic fragments of the molecule. *Nature* **309,** 30–33 (1984).
103. Van Den Bulcke, A. I. *et al.* Structural and Rheological Properties of Methacrylamide Modified Gelatin Hydrogels. (2000). doi:10.1021/BM990017D
104. Carter, S.-S. D. Development of bioprinting platforms for bioartifical pancreas constructs. (2017).
105. Efrat, S. *et al.* Beta-cell lines derived from transgenic mice expressing a hybrid insulin gene-oncogene. *Proc. Natl. Acad. Sci. U. S. A.* **85,** 9037–41 (1988).
106. Poitout, V. *et al.* Morphological and functional characterization of beta TC-6 cells--an insulin-secreting cell line derived from transgenic mice. *Diabetes* **44,** 306–313 (1995).
107. Perelis, M. *et al.* Pancreatic β cell enhancers regulate rhythmic transcription of genes controlling insulin secretion. *Science* **350,** aac4250 (2015).
108. Kang, S., Park, H. S., Jung, H. S. & Park, K. S. Effective revascularisation and enhancement of islet engraftment by cotransplantation of islets with endothelial progenitor cells. *Diabetologia* **53,** S60 (2010).
109. Kang, S. *et al.* Endothelial progenitor cell cotransplantation enhances islet engraftment by

rapid revascularization. *Diabetes* **61,** 866–876 (2012).

110. Penko, D. *et al.* Endothelial progenitor cells enhance islet engraftment, influence β-cell function, and modulate islet connexin 36 expression. *Cell Transplant.* **24,** 37–48 (2015).
111. Peiris, H., Bonder, C. S., Coates, P. T. H., Keating, D. J. & Jessup, C. F. The β-cell/EC axis: how do islet cells talk to each other? *Diabetes* **63,** 3–11 (2014).
112. Sigrist, S. *et al.* Influence of VEGF on the Viability of Encapsulated Pancreatic Rat Islets after Transplantation in Diabetic Mice. *Cell Transplant.* **12,** 627–635 (2003).
113. Ishihara, H. *et al.* Pancreatic beta cell line MIN6 exhibits characteristics of glucose metabolism and glucose-stimulated insulin secretion similar to those of normal islets. *Diabetologia* **36,** 1139–1145 (1993).
114. Komatsu, H. *et al.* Oxygen environment and islet size are the primary limiting factors of isolated pancreatic islet survival. *PLoS One* **12,** e0183780 (2017).
115. Borg, D. J. *et al.* Macroporous biohybrid cryogels for co-housing pancreatic islets with mesenchymal stromal cells. *Acta Biomater.* **44,** 178–187 (2016).
116. Toso, C. *et al.* Human islet transplantation network for the treatment of Type I diabetes: first data from the Swiss-French GRAGIL consortium (1999-2000). *Diabetologia* **44,** 859–864 (2001).
117. Marchioli, G. *et al.* Hybrid Polycaprolactone/Alginate Scaffolds Functionalized with VEGF to Promote de Novo Vessel Formation for the Transplantation of Islets of Langerhans. *Adv. Healthc. Mater.* **5,** 1606–1616 (2016).
118. Agulnick, A. D. *et al.* Insulin-Producing Endocrine Cells Differentiated In Vitro From Human Embryonic Stem Cells Function in Macroencapsulation Devices In Vivo. *Stem Cells Transl. Med.* **4,** 1214–1222 (2015).
119. Robert, T. *et al.* Functional Beta Cell Mass from Device-Encapsulated hESC-Derived Pancreatic Endoderm Achieving Metabolic Control. *Stem Cell Reports* **10,** 739–750 (2018).
120. Kim, Y. *et al.* Islet-like organoids derived from human pluripotent stem cells efficiently function in the glucose responsiveness in vitro and in vivo. *Sci. Rep.* (2016). doi:10.1038/srep35145

121. Servier Smart Medical Art. "Pancreas - Islet of Langerhans" derived from: https:// smart.servier.com/smart_image/islet-of-langerhans-2/ Last accessed on: 22-06-2018. Licensed under a Creative Commons Attribution 3.0 Unported License. *Only the graphic representation of the islet has been used, in its original shape, colour and form without adaptation. All additional mark-up, text and images have been added by the author of this thesis.*

Appendices

Appendix 1: Supplementary Figures

Supplementary Figure 1:

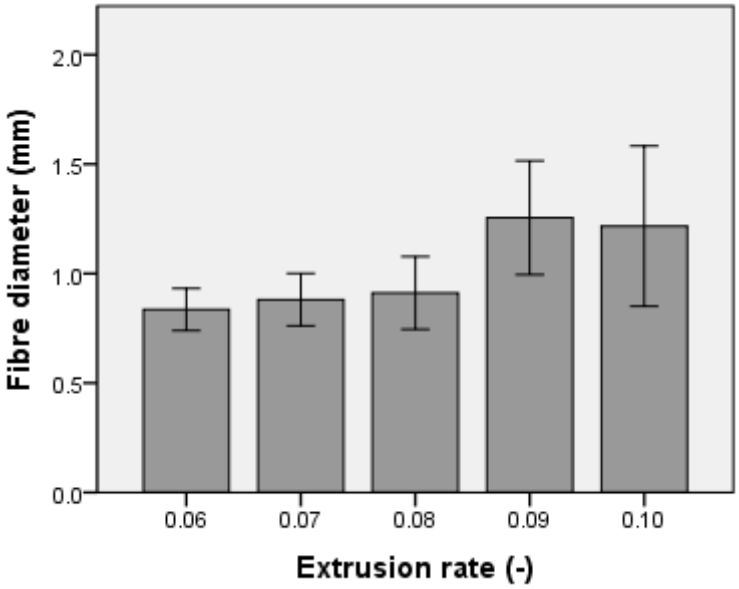

Fig. S1: Fibre diameters of extruded Pluronic F-127 fibres with a 1:1 core/shell ratio at various extrusion rates. Feed rate 400 mm/min with a build plate distance of 0.9 mm. Error bars represent 95% CI, N = 6. In later prints, relying on more suitable core/shell-extrusion ratios, consistency in fibre diameters was still further improved.

Supplementary Figure 2:

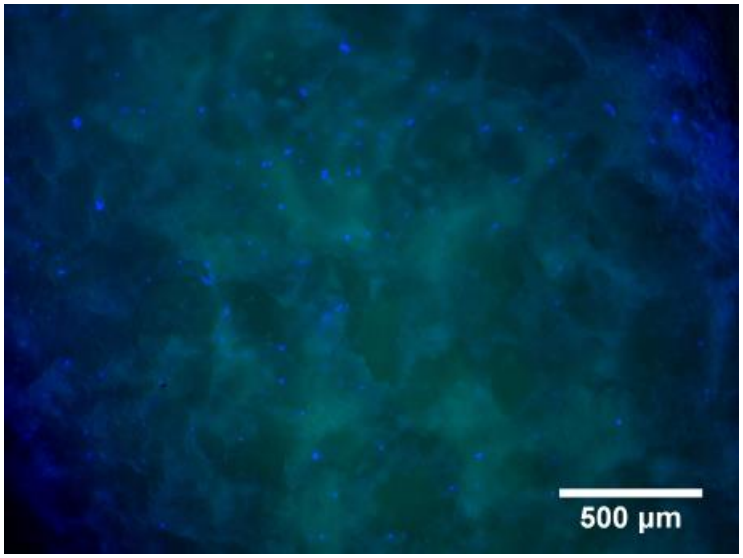

Fig. S2: Co-axially printed fibre with encapsulated MS1 endothelial and β-TC-6 cells. Stained with DAPI (blue) and FITC-labelled anti-CD31 antibodies (green). There is substantial blue staining, indicating presence of cells. However, there is no green staining, with the exception of some very subtle background noise, indicating no CD31-positive cells. This may either indicate there are no MS1 cells present or MS1 cells have lost CD31-expression. Both are unlikely, it is therefore thought that staining procedure has failed due to some unknown reason. Time was too limited for extensive trouble-shooting and this question remains to be answered.

Supplementary Figure 3:

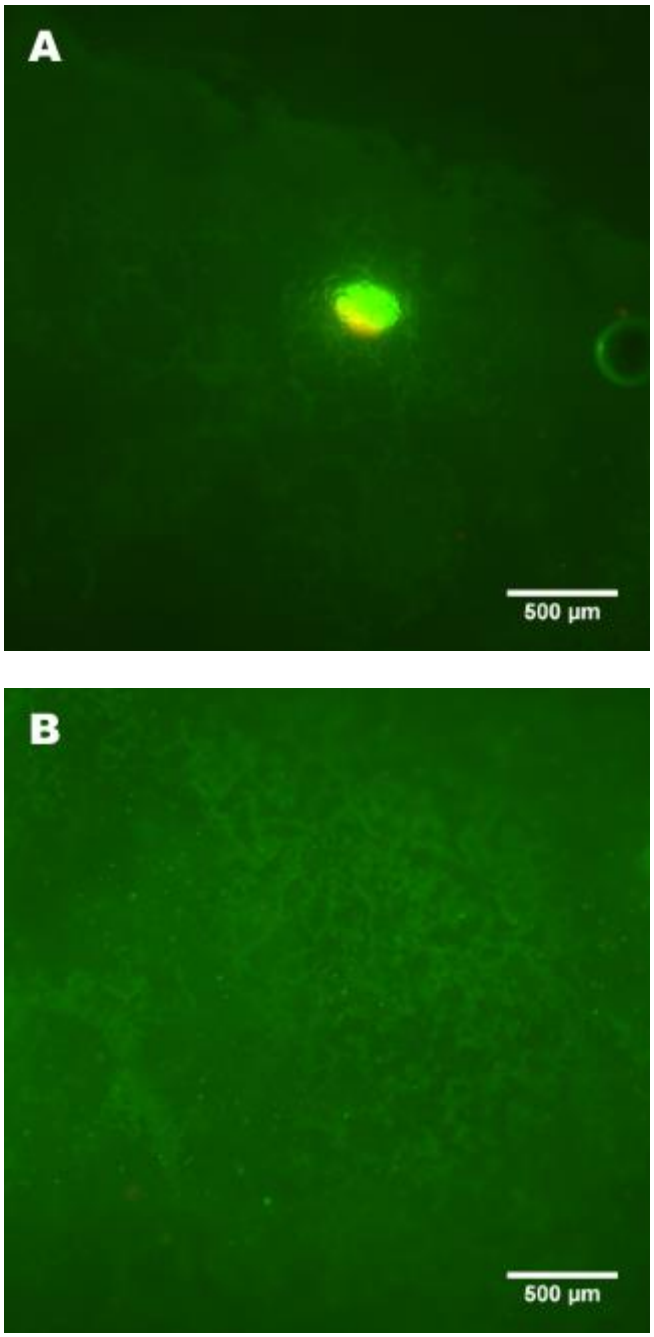

Fig. S3: Original microscopy images without noise filtering, exemplified by islets only at t = 1 days (**A**) and EPCs only at t = 1 days (**B**), corresponding to **Fig. 14A** and **14B** in the main text, respectively. The same noise filters have been applied to all images in **Fig. 14** and **Fig. 15** in the main text, in order to visualise some images more clearly without altering the general representation in the images.

Supplementary Figure 4:

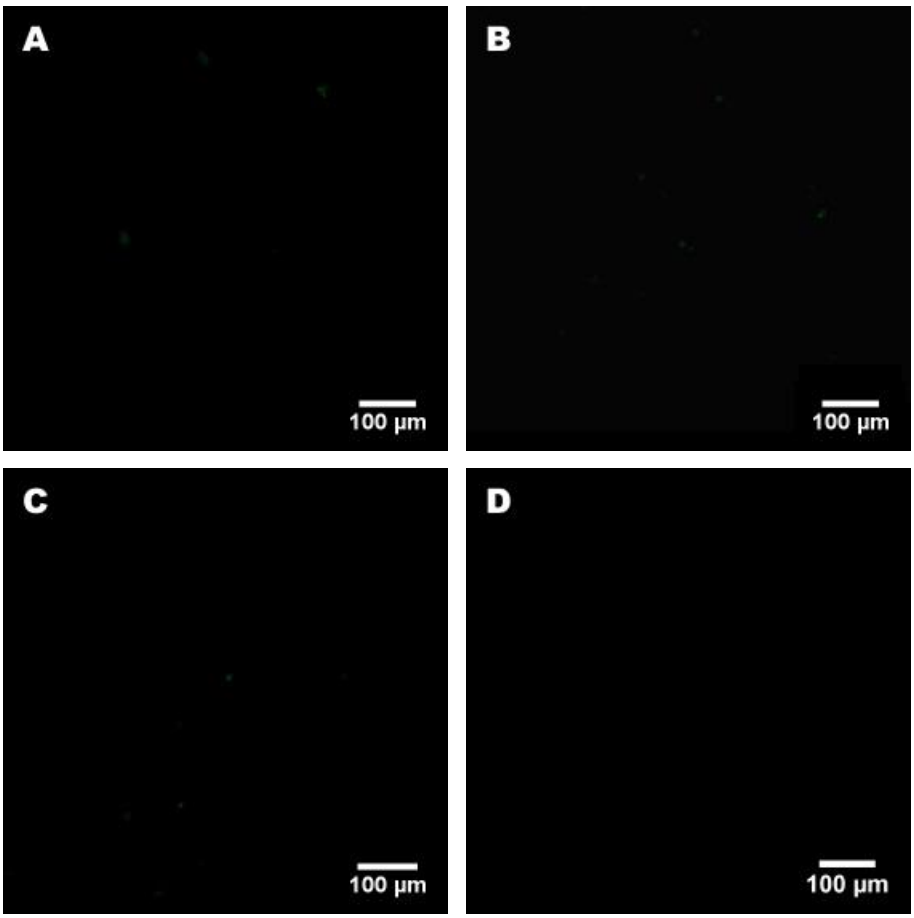

Fig. S4A-C: Examples of pictures of EPCs cultured in scaffolds with hypoxia with boosted contrast in imaging software. When close attention is paid to the images, faint green spots can be detected in all three images. **B** is derived from **Fig. 17C**.

Fig. S4D: An example of negative control (normoxia) with the same boosted contrast. No green spots can be observed. Derived from **Fig. 17B**.

Appendix 2: G-codes for prints

All G-codes for prints in this thesis were coded manually without CAD or slicing software. The codes have been provided below.

Pluronic fibre printing with extrusion ratio 4 : 96

```
;(setup code)
;(relative positioning, mm, go to start, feed)
G21
G91
G92 E0
G0 Z0.7 F400
G0 X10 E0.6 A0.5 B0.5;                                  start 1cm extrusion
G1 X50 E0.5890486284385725 A0.96 B0.04;                 first line
G1 X5 E0.05890486284385725 A0.96 B0.04
F300;                                                   corner right side
G1 X5 E0.05890486284385725 A0.96 B0.04
G1 Y-4 E0.011780972568771449 A0.96 B0.04
G1 X-5 E0.05890486284385725 A0.96 B0.04
F400;                                                   second line
G1 X-50 E0.5890486284385725 A0.96 B0.04
F300;                                                   corner left side
G1 X-5 E0.05890486284385725 A0.96 B0.04
G1 Y-4 E0.011780972568771449 A0.96 B0.04
G1 X5 E0.05890486284385725 A0.96 B0.04
F400;                                                   third line
G1 X50 E0.5890486284385725 A0.96 B0.04
F300
G1 X5 E0.05890486284385725 A0.96 B0.04
G1 Y-4 E0.011780972568771449 A0.96 B0.04
G1 X-5 E0.05890486284385725 A0.96 B0.04
F400;                                                   fourth line
G1 X-50 E0.5890486284385725 A0.96 B0.04
F300
G1 X-5 E0.05890486284385725 A0.96 B0.04
G1 Y-4 E0.011780972568771449 A0.96 B0.04
G1 X5 E0.05890486284385725 A0.96 B0.04
F400;                                                   fifth line
G1 X50 E0.5890486284385725 A0.96 B0.04
F300
G1 X5 E0.05890486284385725 A0.96 B0.04
G1 Y-4 E0.011780972568771449 A0.96 B0.04

G0 Z20 E-0.5 A0.5 B0.5
G0 Y80
```

Pluronic fibre printing with extrusion ratio 16 : 84

```
;(setup code)
;(relative positioning, mm, go to start, feed)
G21
G91
G92 E0
G0 Z0.7 F400
G0 X10 E0.6 A0.5 B0.5;                                  start 1cm extrusion
G1 X50 E0.5890486284385725 A0.84 B0.16;                 first line
G1 X5 E0.05890486284385725 A0.84 B0.16
F300;                                                   corner right side
G1 X5 E0.05890486284385725 A0.84 B0.16
G1 Y-4 E0.011780972568771449 A0.84 B0.16
G1 X-5 E0.05890486284385725 A0.84 B0.16
F400;                                                   second line
G1 X-50 E0.5890486284385725 A0.84 B0.16
F300;                                                   corner left side
G1 X-5 E0.05890486284385725 A0.84 B0.16
G1 Y-4 E0.011780972568771449 A0.84 B0.16
G1 X5 E0.05890486284385725 A0.84 B0.16
F400;                                                   third line
G1 X50 E0.5890486284385725 A0.84 B0.16
F300
G1 X5 E0.05890486284385725 A0.84 B0.16
G1 Y-4 E0.011780972568771449 A0.84 B0.16
G1 X-5 E0.05890486284385725 A0.84 B0.16
F400;                                                   fourth line
G1 X-50 E0.5890486284385725 A0.84 B0.16
F300
G1 X-5 E0.05890486284385725 A0.84 B0.16
G1 Y-4 E0.011780972568771449 A0.84 B0.16
G1 X5 E0.05890486284385725 A0.84 B0.16
F400;                                                   fifth line
G1 X50 E0.5890486284385725 A0.84 B0.16
F300
G1 X5 E0.05890486284385725 A0.84 B0.16
G1 Y-4 E0.011780972568771449 A0.84 B0.16

G0 Z20 E-0.5 A0.5 B0.5
G0 Y80
```

GelMA/Alginate fibres with MS1 and β-TC-6 cells or labelled GelMA in core

```
;(setup code)
;(relative positioning, mm, go to start, feed)
G21
G91
G92 E0
G0 Z0.7 F400
G1 X10 E1 A0.75 B0.25;                                  start 1cm extrusion
G1 X60 E0.60 A0.75 B0.25;                               first line

G1 Y-4 E0.020 A0.75 B0.25

G1 X-60 E0.60 A0.75 B0.25
G1 Y-4 E0.020 A0.75 B0.25
G1 X60 E0.60 A0.75 B0.25

G1 Y-4 E0.020 A0.75 B0.25
G1 X-60 E0.60 A0.75 B0.25

G1 Y-4 E0.020 A0.75 B0.25
G1 X60 E0.60 A0.75 B0.25

G1 Y-4 E0.020 A0.75 B0.25

G0 F600
G0 Z20 E-0.5; A0.75 B0.25
G0 Y80
```

3D-constructs

First layer “x”

```
;(setup code)
;(relative positioning, mm, go to start, feed)
G21
G91
G92 E0
G0 Z0.7 F400
G1 X10 E0.25 A0.75 B0.25;                                   start 1cm extrusion
G1 X10 E0.25 A0.75 B0.25;                                   start 1cm extrusion
G1 X10 E0.12 A0.75 B0.25;                                   start 1cm extrusion
G1 X10 E0.12 A0.75 B0.25;                                   start 1cm extrusion

G1 X16 E0.12 A0.75 B0.25;                                   first line

G1 Y-4 E0.030 A0.75 B0.25

G1 X-16 E0.12 A0.75 B0.25
G1 Y-4 E0.030 A0.75 B0.25
G1 X16 E0.12 A0.75 B0.25

G1 Y-4 E0.030 A0.75 B0.25
G1 X-16 E0.12 A0.75 B0.25

G1 Y-4 E0.030 A0.75 B0.25
G1 X16 E0.12 A0.75 B0.25

G1 Y-4 E0.030 A0.75 B0.25

G0 F600
G0 Z20 E-0.5; A0.75 B0.25
G0 Y80
```

First layer "y"

```
;(setup code)
;(relative positioning, mm, go to start, feed)
G21
G91
G92 E0
G0 Z0.7 F400
G1 X10 E0.25 A0.75 B0.25;                                   start 1cm extrusion
G1 X10 E0.25 A0.75 B0.25;                                   start 1cm extrusion
G1 X10 E0.12 A0.75 B0.25;                                   start 1cm extrusion
G1 X10 E0.12 A0.75 B0.25;
G1 Y-16 E0.12 A0.75 B0.25;                                  first line

G1 X4 E0.030 A0.75 B0.25

G1 Y16 E0.12 A0.75 B0.25
G1 X4 E0.030 A0.75 B0.25
G1 Y-16 E0.12 A0.75 B0.25

G1 X4 E0.030 A0.75 B0.25
G1 Y16 E0.12 A0.75 B0.25

G1 X4 E0.030 A0.75 B0.25
G1 Y-16 E0.12 A0.75 B0.25

G1 X4 E0.030 A0.75 B0.25
G1 Y-4 E0.030 A0.75 B0.25

G0 F600
G0 Z20 E-0.5; A0.25 B0.25
G0 Y80
```

G-codes for the consecutive layers in x and y can be obtained by changing the z-offset from 0.7 to 1.2 and 1.5 for both x and y for a total construct of six layers. All G-codes above were optimised for the smaller nozzle types, the next G-codes used in islet printing experiments used the larger nozzle types.

Islet print G-codes

Layer in “x”

```
;(setup code)
;(relative positioning, mm, go to start, feed)
G21
G91
G92 E0
G0 Z0.7 F400
G1 X10 E0.25 A0.75 B0.25;                                   start 1cm extrusion
G1 X10 E0.25 A0.75 B0.25;                                   start 1cm extrusion
G1 X10 E0.25 A0.75 B0.25;                                   start 1cm extrusion
G1 X10 E0.12 A0.75 B0.25;                                   start 1cm extrusion
G1 X10 E0.12 A0.75 B0.25;                                   start 1cm extrusion

G1 X20 E0.20 A0.75 B0.25;                                   first line

G1 Y-5 E0.05 A0.75 B0.25

G1 X-20 E0.20 A0.75 B0.25
G1 Y-5 E0.05 A0.75 B0.25
G1 X20 E0.20 A0.75 B0.25

G1 Y-5 E0.05 A0.75 B0.25
G1 X-20 E0.20 A0.75 B0.25

G1 Y-5 E0.05 A0.75 B0.25
G1 X20 E0.20 A0.75 B0.25

G1 Y-5 E0.05 A0.75 B0.25

G0 F600
G0 Z20 E-0.5; A0.75 B0.25
G0 Y80
```

Layer in “y”

```
;(setup code)
;(relative positioning, mm, go to start, feed)
G21
G91
G92 E0
G0 Z0.7 F400
G1 X10 E0.25 A0.75 B0.25;                                   start 1cm extrusion
G1 X10 E0.25 A0.75 B0.25;                                   start 1cm extrusion
G1 X10 E0.25 A0.75 B0.25;                                   start 1cm extrusion
G1 X10 E0.12 A0.75 B0.25;                                   start 1cm extrusion
G1 X10 E0.12 A0.75 B0.25;
G1 Y-20 E0.20 A0.75 B0.25;                                  first line

G1 X5 E0.05 A0.75 B0.25

G1 Y20 E0.20 A0.75 B0.25
G1 X5 E0.05 A0.75 B0.25
G1 Y-20 E0.20 A0.75 B0.25

G1 X5 E0.05 A0.75 B0.25
G1 Y20 E0.20 A0.75 B0.25

G1 X5 E0.05 A0.75 B0.25
G1 Y-20 E0.20 A0.75 B0.25

G1 X4 E0.05 A0.75 B0.25
G1 Y-4 E0.05 A0.75 B0.25

G0 F600
G0 Z20 E-0.5; A0.25 B0.25
G0 Y80
```

Appendix 3: Biofabrication Double Degree First Thesis – Utrecht University

The document in the Appendix below is the manuscript that was completed at Utrecht University as a part of the Biofabrication Double Degree (see Biofabrication Double Degree statement at the beginning of this thesis). It is included for reference, but should not be taken into further account for the review of this thesis as it has already been reviewed in a separate procedure at Utrecht University.